

Homogenization of the vibro–acoustic transmission on perforated plates

E. Rohan^{a,*}, V. Lukeš^a

^a*European Centre of Excellence, NTIS New Technologies for Information Society,
Faculty of Applied Sciences,
University of West Bohemia,
Univerzitní 22, 30614 Plzeň, Czech Republic*

Abstract

The paper deals with modelling of acoustic waves which propagate in inviscid fluids interacting with perforated elastic plates. The plate can be replaced by an interface on which transmission conditions are derived by homogenization of a problem describing vibroacoustic fluid-structure interactions in a transmission layer in which the plate is embedded. The Reissner-Mindlin theory of plates is adopted for periodic perforations designed by arbitrary cylindrical holes with axes orthogonal to the plate midplane. The homogenized model of the vibroacoustic transmission is obtained using the two-scale asymptotic analysis with respect to the layer thickness which is proportional to the plate thickness and to the perforation period. The nonlocal, implicit transmission conditions involve a jump in the acoustic potential and its normal one-side derivatives across the interface which represents the plate with a given thickness. The homogenized model was implemented using the finite element method and validated using direct numerical simulations of the non-homogenized problem. Numerical illustrations of the vibroacoustic transmission are presented.

Keywords: Vibro-acoustic transmission, perforated plate, thin layer, two scale homogenization, Helmholtz equation, finite element method

1. Introduction

The noise and vibration reduction belongs to important issues in design of structures used in the automotive industry, or civil engineering. The engine silencer used to reduce the noise emitted by the exhaust gas presents

*Corresponding author

Email addresses: rohan@kme.zcu.cz (E. Rohan), vlukes@kme.zcu.cz (V. Lukeš)

an important and well known example. However, there are many similar solid structures which can influence the acoustic wave propagation in fluid. Usually they involve porous, or perforated plates, or panels, such that they are permeable for the gas flow. The straightforward approach to modelling the acoustic wave propagation through vibrating perforated plates consists in solving directly the vibroacoustic problem with a 3D elastic structure describing the plate. However, its numerical treatment using the finite element method can lead to an intractable problem because of the prohibitive number of DOFs corresponding to the geometric complexity of the perforated structure. Therefore, it is reasonable to replace the elastic plate by an interface on which coupling transmission conditions are prescribed.

In this paper, we consider the acoustic wave propagation in an inviscid fluid interacting with elastic structures designed as periodically perforated plates. The aim is to derive non-local vibro-acoustic transmission conditions using the periodic homogenization method. Although similar problems have been treated in the literature, cf. [6], in this context, the plate elasticity has not been considered yet. As for the rigid structures, semi-empirical formulae for the acoustic impedance exist which were tuned by experiments, or developed using the electro-acoustic equivalent circuit theory [8, 19, 20], or the Helmholtz-Kirchhoff integral theory [23]. During the last decade, a number of works appeared which are based on a homogenization strategy. For a thin rigid perforated plate represented by interface Γ_0 and characterized by the thickness $\approx \delta$ it has been shown in [1, 6] that this interface is totally transparent for the acoustic field at the zero order δ^0 terms of the model which describes the limit behaviour for $\delta \rightarrow 0$, cf. [7]. For a higher order approximation, an approach based on the so-called inner and outer asymptotic expansions has been developed, such that two associated acoustic fields are coupled, one being relevant in the proximity of the perforations, the other at a distance from the limit interface, see *e.g.* [5, 10, 11]. In contrast with [1] dealing with thin perforated interfaces only, in [14] we were concerned with homogenization of a fictitious layer in which rigid periodically distributed obstacles were placed. In particular, a rigid plate perforated by arbitrary shaped pores could be considered. Therein nonlocal transmission conditions were obtained as the two-scale homogenization limit of a standard acoustic problem imposed in the layer.

Here we follow the approach reported in [14] to develop vibroacoustic transmission conditions which substitute the vibroacoustic interaction on an elastic perforated plate immersed in the acoustic fluid. Up to our knowledge, despite some numerical studies, see *e.g.* [21], a rigorous treatment of such a problem has not been treated using the homogenization method so far. As the result we obtain vibroacoustic transmission conditions in a form of

an implicit Dirichlet-to-Neumann operator. Due to this operator, the elastic perforated plate can be replaced by an interface on which a jump of the global acoustic pressure is linked to the acoustic momenta associated with two faces of the homogenized plate. It allows us to obtain an efficient numerical model which takes into account geometrical details of the periodic perforation without need of discretizing the vibroacoustic problem at the global level. In other words, the homogenized interface provides a reduced model in which a complex 3D elastic structure is replaced by a 2D perforated plate model whose coefficients retain information about the perforation geometry. To do so, we rely on the homogenized Reissner-Mindlin plate tailor-made for the “simple” perforation represented by general cylindrical holes with axes orthogonal to the mid-plane of the plate. Elastic strongly heterogeneous plates were treated in [17, 18] where the framework of the Reissner-Mindlin theory was used to derive a model of phononic plates, cf. [13], but without the interaction with an exterior acoustic field.

The proposed modelling conception based on the problem decomposition and using the homogenization provides an alternative framework for modelling of microporous panels which are known for their capabilities of acoustic attenuation [22, 23, 9]. In [12] the so-called patch transfer functions were developed for numerical modelling of compliant micro-perforated panels.

The plan of the paper is as follows. In Section 2 the vibroacoustic problem of the wave propagation in a waveguide containing the perforated plate is decomposed into the problem in a fictitious transmission layer (the “in-layer” problem) and the “outer” problem governing the acoustic field out of the layer. The “in-layer” vibroacoustic problem is treated using the homogenization method in Section 3, where the local problems imposed in the representative periodic cell are introduced and formulae for the homogenized coefficients are given. In Section 4, as the main result of this paper, the global acoustic problem is established using the limit “in-layer” and the “outer” problems which are coupled using additional conditions derived by an additional integration and averaging procedure. The limit two-scale model of the homogenized layer is validated in Section 5 using direct numerical simulations of the original problem. Finally, in Section 6, the proposed model is employed to simulate wave propagation in a waveguide equipped with the perforated plate. Some technical auxiliary derivations are presented in the Appendix.

Notation. In the paper, the mathematical models are formulated in a Cartesian coordinate system $\mathcal{R}(O; \mathbf{e}_1, \mathbf{e}_2, \mathbf{e}_3)$ where O is the origin of the space and $(\mathbf{e}_1, \mathbf{e}_2, \mathbf{e}_3)$ is a orthonormal basis for this space. The spatial position x in the medium is specified through the coordinates (x_1, x_2, x_3) with re-

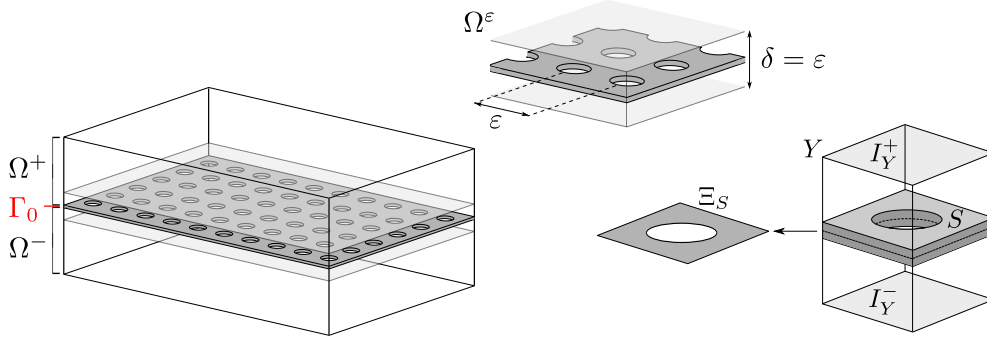


Figure 1: Left: The global domain decomposition into Ω^+ and Ω^- separated by the homogenized perforated plate represented by the interface Γ_0 . Center: detail of the layer structure; the layer thickness is proportional to the plate thickness and to the perforation period. Right: perforated interface and the representative periodic cell $Y = Y^* \cup \bar{S}$.

spect to a Cartesian reference frame \mathcal{R} . The boldface notation for vectors, $\mathbf{a} = (a_i)$, and for tensors, $\mathbf{b} = (b_{ij})$, is used. The gradient and divergence operators applied to a vector \mathbf{a} are denoted by $\nabla \mathbf{a}$ and $\nabla \cdot \mathbf{a}$, respectively. By $\nabla^S \mathbf{u}$ we denote the symmetrized gradient $\nabla \mathbf{u}$, *i.e.* the strain tensor. When these operators have a subscript which is space variable, it is for indicating that the operator acts relatively at this space variable, for instance $\nabla_x = (\partial_i^x)$. The symbol dot ‘ \cdot ’ denotes the scalar product between two vectors and the symbol colon ‘ $:$ ’ stands for scalar (inner) product of two second-order tensors. Throughout the paper, x denotes the global (“macroscopic”) coordinates, while the “local” coordinates y describe positions within the representative unit cell $Y \subset \mathbb{R}^3$ where \mathbb{R} is the set of real numbers. By latin subscripts $i, j, k, l \in \{1, 2, 3\}$ we refer to vectorial/tensorial components in \mathbb{R}^3 , whereas subscripts $\alpha, \beta \in \{1, 2\}$ are reserved for the tangential components with respect to the plate midsurface, *i.e.* coordinates x_α of vector represented by $x' = (x_1, x_2) = (x_\alpha)$ are associated with directions $(\mathbf{e}_1, \mathbf{e}_2)$. Moreover, $\bar{\nabla}_x = (\partial_\alpha)$ is the “in-plane” gradient. The gradient in the so-called dilated configuration with coordinates (x', z) is denoted by $\hat{\nabla} = (\bar{\nabla}, \frac{1}{\varepsilon} \partial_z)$. We also use the jump w.r.t. the transversal coordinate, $\llbracket q(\cdot, x_3) \rrbracket_r^\pm = q(\cdot, r/2) - q(\cdot, -r/2)$.

2. Formulation and decomposition of the vibroacoustic transmission problem

The aim of the paper is to find a representation of the vibro-acoustic interaction on a perforated plate. For this, homogenized vibroacoustic transmission conditions are derived using the asymptotic analysis w.r.t. a scale

parameter ε which has a double role: on one hand it deals with the thickness of an elastic plate when considered as a 3D object, on the other hand it describes the size and spacing of holes periodically drilled in the plate structure.

The flowchart of deriving the transmission conditions for a limit global problem consists of the following steps:

- The vibro-acoustic problem (later called the “global problem”) is formulated in a domain $\Omega^G \subset \mathbb{R}^3$ in which the perforated elastic plate is embedded, being represented by a planar surface – the plate midsurface.
- A transmission layer Ω_δ of the thickness δ is introduced in terms of Γ_0 which constitutes its midsurface. This will allow to decompose the global problem into two subproblems: the vibroacoustic interaction in the layer Ω_δ and the outer acoustic problems in $\Omega^G \setminus \Omega_\delta$. The two subproblems are coupled by natural transmission conditions on the “fictitious” interfaces Γ_δ^\pm .
- We consider the layer thickness being proportional to the scale parameter, thus, $\delta = \varkappa\varepsilon$, where $\varkappa > 0$ is fixed. The asymptotic analysis $\delta \approx \varepsilon \rightarrow 0$ considered for the problem in Ω_δ with the Neumann type boundary conditions on Γ_δ^\pm leads to the homogenized vibroacoustic transmission problem defined on Γ_0 . In this analysis, ε has the double role announced above and the plate is described using its 2D representation in the framework of the Reissner-Mindlin plate theory. In Remark 1 we explain the dual interpretation of the plate thickness used in the asymptotic analysis of the vibro-acoustic problem.
- The final step is to derive the limit global problem for the acoustic waves in the fluid interacting with the homogenized perforated plate represented by Γ_0 . For this, with a few modifications we follow the approach used in [14], where the rigid plate was considered; a given plate thickness h corresponds to given finite thickness δ_0 of the transmission layer. Then the continuity of the acoustic fields on interfaces $\Gamma_{\delta_0}^\pm$ yields the homogenized vibroacoustic transmission conditions which hold on Γ_0 .

2.1. Global problem with transmission layer

In this section, we introduce the problem of acoustic waves in a domain Ω^G with embedded perforated elastic plate Σ^ε , see Fig. 2 and Fig. 3. The

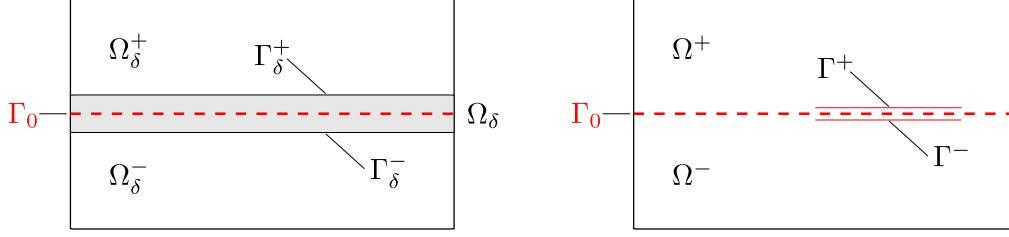


Figure 2: Left: Transmission layer Ω_δ of thickness δ embedded in the global domain Ω^G . Right: Interface Γ_0 representing the homogenized transmission layer.

acoustic fluid occupies the domain $\Omega^{*\varepsilon}$. We consider a fictitious transmission layer Ω_δ with a thickness $\delta > 0$, such that $\Sigma^\varepsilon \subset \Omega_\delta$. The plate thickness is $h^\varepsilon = \varepsilon \bar{h}$, while the layer thickness $\delta = \varkappa \varepsilon$ for a given fixed $\varkappa > 0$.

For a fixed parameter $\varepsilon > 0$, correspondingly to $\Omega^{*\varepsilon}$ and Σ^ε , we use a simplified notation Ω^* and Σ . The acoustic harmonic wave with the frequency ω is described by the acoustic potential $p : \Omega^* \ni x \mapsto \mathbb{R}^3$ in the fluid, the corresponding wave in the elastic body is described by the displacement field $\mathbf{u} : \Sigma \ni x \mapsto \mathbb{R}^3$. Assuming the body is fixed to a rigid frame on the boundary $\partial_u \Sigma$ and interacting with the fluid on $\partial_* \Sigma = \partial \Sigma \setminus \partial_u \Sigma$, these fields satisfy the following equalities:

$$\begin{aligned} c^2 \nabla^2 p + \omega^2 p &= 0 & \text{in } \Omega^* , \\ \nabla \cdot \boldsymbol{\sigma}(\mathbf{u}) + \omega^2 \rho \mathbf{u} &= 0 & \text{in } \Sigma , \\ \text{acoustic transmission:} \\ \left. \begin{aligned} i\omega \mathbf{n} \cdot \mathbf{u} &= \mathbf{n} \cdot \nabla p \\ \mathbf{n} \cdot \boldsymbol{\sigma}(\mathbf{u}) &= \mathbf{b}(p) = i\omega \rho_0 p \mathbf{n} \end{aligned} \right\} & \text{on } \partial_* \Sigma , \end{aligned}$$

incident, or reflected acoustic waves in the fluid:

$$ri\omega c p + c^2 \frac{\partial p}{\partial n} = s 2i\omega c \bar{p} \quad \text{on } \partial_{\text{ext}} \Omega^G \setminus \partial_u \Sigma ,$$

clamped elastic structure:

$$\mathbf{u} = 0 \quad \text{on } \partial_u \Sigma . \tag{1}$$

Above, c is the sound speed in the acoustic fluid, $\boldsymbol{\sigma}(\mathbf{u})$ is the stress in the linear elastic solid, ρ_0 is reference fluid density, and by $\mathbf{n} = (n_i)$ we denote the normal vector. The constants $r, s \in \{0, 1\}$ and \bar{p} are defined to describe incident, reflected, or absorbed acoustic waves in the fluid, according to a selected part of the boundary.

2.2. Geometry of the perforated layer

Given a bounded 2D manifold $\Gamma_0 \subset \{x \in \Omega^G | x_3 = 0\}$ representing the plate mid-plane, we introduce $\Omega_\delta = \Gamma_0 \times]-\delta/2, \delta/2[\subset \Omega^G$, an open domain representing the transmission layer. This enables to decompose Ω^G into three nonoverlapping parts, as follows: $\Omega^G = \Omega_\delta \cup \Omega_\delta^+ \cup \Omega_\delta^-$. Thus, the transmission layer is bounded by $\partial\Omega_\delta$ which splits into three parts:

$$\partial\Omega_\delta = \Gamma_\delta^+ \cup \Gamma_\delta^- \cup \partial_{\text{ext}}\Omega_\delta, \quad \Gamma_\delta^\pm = \Gamma_0 \pm \frac{\delta}{2}\vec{e}_3, \quad \partial_{\text{ext}}\Omega_\delta = \partial\Gamma_0 \times]-\delta/2, \delta/2[, \quad (2)$$

where $\delta > 0$ is the layer thickness and $\vec{e}_3 = (0, 0, 1)$, see Fig. 1. In the context of the transmission layer definition, we consider the plate as a 3D domain Σ^ε defined in terms of the perforated midsurface Γ^ε ; the following definitions are employed:

$$\begin{aligned} \Sigma^\varepsilon &= \Gamma^\varepsilon \times \varepsilon\bar{h}] - 1/2, +1/2[, \\ \partial\Sigma^\varepsilon &= \partial_o\Sigma^\varepsilon \cup \partial_+\Sigma^\varepsilon \cup \partial_-\Sigma^\varepsilon \cup \partial_u\Sigma^\varepsilon, \end{aligned} \quad \text{where} \quad (3)$$

$$\begin{aligned} \partial_o\Sigma^\varepsilon &= \partial_o\Gamma^\varepsilon \times \varepsilon\bar{h}] - 1/2, +1/2[, \\ \partial_\pm\Sigma^\varepsilon &= \Gamma^\varepsilon \pm \varepsilon\bar{h}/2, \end{aligned}$$

where $\partial_u\Sigma^\varepsilon$ is the surface where the plate is clamped.

The midsurface Γ^ε representing the perforated plate is generated using a representative cell $\Xi_S \subset \mathbb{R}^2$, as a periodic lattice. Let $\Xi =]0, \ell_1[\times]0, \ell_2[$, where $\ell_1, \ell_2 > 0$ are given (usually $\ell_1 = \ell_2 = 1$) and consider the hole $\Xi^* \subset \Xi$, whereas its complement $\Xi_S = \Xi \setminus \Xi^*$ defines the solid plate segment. Then

$$\Gamma^\varepsilon = \bigcup_{k \in \mathbb{Z}^2} \varepsilon \left(\Xi_K + \sum_{i=1,2} k_i \ell_i \vec{e}_i \right) \cap \Gamma_0, \quad (4)$$

Further we introduce the representative periodic cell Y and define its solid part $S \subset Y$,

$$\begin{aligned} Y &= \Xi \times]-\varkappa/2, +\varkappa/2], \\ S &= \Xi_S \times \bar{h}] - 1/2, +1/2[, \end{aligned} \quad (5)$$

so that $Y^* = Y \setminus \bar{S}$ is the fluid part. Obviously, in the transmission layer Ω_δ , the fluid occupies the part

$$\Omega^{*\varepsilon} = \bigcup_{k \in \mathbb{Z}^2} \varepsilon(Y^* + \sum_{i=1,2} k_i \ell_i \vec{e}_i) \cap \Omega_\delta, \quad (6)$$

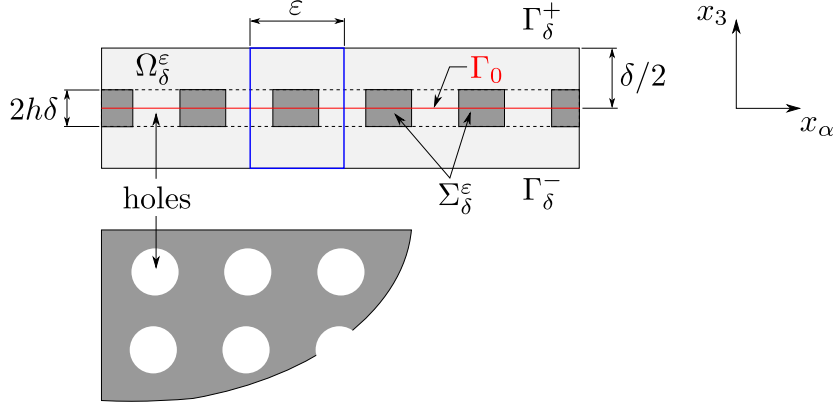


Figure 3: Scheme of the transmission layer Ω_δ in which the perforated plate Σ_δ^ϵ (dark gray) is embedded. The complementary domain Ω_δ^ϵ is occupied by the acoustic fluid (light gray).

where $\vec{e}_1 = (1, 0, 0)$ and $\vec{e}_2 = (0, 1, 0)$.

For completeness, by virtue of (3) we can introduce the decomposition of boundary $\partial S = \partial_o S \cup \partial_\pm S \cup \partial_\# S$. For this we need the boundary $\partial \Xi_S = \partial_o \Xi_S \cup \partial_\# \Xi_S$, where $\partial_\# \Xi_S \equiv \partial \Xi$, so that the closed curve $\partial_o \Xi_S = \partial \Xi^*$ generates the cylindrical boundary $\partial_o S$:

$$\begin{aligned} \partial_o S &= \partial_o \Xi_S \times [\bar{h}] - 1/2, +1/2[, \\ \partial_\pm S &= \Xi_S \pm \vec{e}_3 \bar{h}/2 , \\ \partial_\# S &= \partial \Xi \times [\bar{h}] - 1/2, +1/2[. \end{aligned} \tag{7}$$

For the sake of simplicity, by $\partial \Xi_S$ we shall refer to $\partial_o \Xi_S$.

2.3. Problem decomposition

The domain split allows us to decompose problem (1) into three parts. By P^δ we denote the acoustic potential in Ω_δ^+ and Ω_δ^- , whereas p^ϵ is the acoustic potential in the transmission layer Ω_δ , see Fig. 3. Further, by $i\omega g^{\epsilon\pm}$ we denote the acoustic fluid velocity projected into the normal of the interfaces Γ_δ^\pm . The following subproblems are considered:

1,2: Given \hat{p}^ϵ on Γ_δ^\pm , find P^δ defined in $\Omega_\delta^G = \Omega_\delta^+ \cup \Omega_\delta^-$, such that

$$c^2 \nabla^2 P^\delta + \omega^2 P^\delta = 0 \quad \text{in } \Omega_\delta^+ \cup \Omega_\delta^- ,$$

interface condition:

$$P^\delta = \hat{p}^\epsilon \quad \text{on } \Gamma_\delta^\pm , \tag{8}$$

other boundary conditions

$$ri\omega c P^\delta + c^2 \frac{\partial P^\delta}{\partial n} = s2i\omega c \bar{p} \quad \text{on } \partial_{\text{ext}} \Omega_\delta^G ,$$

where $\partial_{\text{ext}}\Omega_\delta^G = \partial\Omega^G \cap (\partial\Omega_\delta^+ \cup \partial\Omega_\delta^-)$ is the “external” boundary. As in problem (1), r and s are constants attaining values 0, or 1, whereas \bar{p} is the amplitude of an incident wave. In the context of a waveguide, we consider $\partial_{\text{ext}}\Omega_\delta^G$ to be decomposed into three parts, $\partial_{\text{in}}\Omega_\delta^G$, $\partial_{\text{out}}\Omega_\delta^G$, and $\partial_w\Omega_\delta^G$, denoting the input, the output and walls, respectively. By the constants r, s in (8)₃ different conditions on $\partial\Omega_\delta^G$ are respected: $r = s = 0$ on the walls $\partial_w\Omega_\delta^G$, whereas $r = s = 1$ on $\partial_{\text{in}}\Omega_\delta^G$ and $r = 1, s = 0$ on $\partial_{\text{out}}\Omega_\delta^G$, which accounts for the non-reflection condition.

3: Given $g^{\varepsilon\pm}$ on Γ_δ^\pm , find p^ε in $\Omega_\delta^{*\varepsilon}$ and \mathbf{u}^ε in Σ^ε , such that

$$\begin{aligned}
& c^2 \nabla^2 p^\varepsilon + \omega^2 p^\varepsilon = 0 \quad \text{in } \Omega_\delta^{*\varepsilon}, \\
& \text{interface conditions} \quad \frac{\partial p^\varepsilon}{\partial n} = -i\omega g^{\varepsilon\pm} \quad \text{on } \Gamma_\delta^\pm, \\
& \nabla \cdot \boldsymbol{\sigma}(\mathbf{u}^\varepsilon) + \omega^2 \rho \mathbf{u}^\varepsilon = 0 \quad \text{in } \Sigma_\delta^\varepsilon, \\
& \text{acoustic transmission:} \\
& \left. \begin{aligned} i\omega \mathbf{n} \cdot \mathbf{u}^\varepsilon &= \mathbf{n} \cdot \nabla p^\varepsilon \\ \mathbf{n} \cdot \boldsymbol{\sigma}(\mathbf{u}^\varepsilon) &= \mathbf{b}(p^\varepsilon) = i\omega \rho_0 p^\varepsilon \mathbf{n} \end{aligned} \right\} \quad \text{on } \partial_* \Sigma_\delta^\varepsilon, \\
& \text{other boundary conditions} \\
& ri\omega c p^\varepsilon + c^2 \frac{\partial p^\varepsilon}{\partial n} = s 2i\omega c \bar{p} \quad \text{on } \partial_{\text{ext}}\Omega_\delta^G \setminus \partial_u \Sigma_\delta^\varepsilon, \\
& \text{clamped elastic structure:} \\
& \mathbf{u}^\varepsilon = 0 \quad \text{on } \partial_u \Sigma_\delta^\varepsilon.
\end{aligned} \tag{9}$$

where $\partial_* \Sigma_\delta^\varepsilon = \partial \Sigma_\delta^\varepsilon \cap \partial \Omega_\delta^{*\varepsilon}$ is the surface of the elastic structure in contact with the fluid, thus, $\partial \Sigma_\delta^\varepsilon = \partial_* \Sigma_\delta^\varepsilon \cup \partial_u \Sigma_\delta^\varepsilon$.

4. For a fixed ε and δ , solutions to problems (8) and (9) are equivalent to the solution of (1), if the coupling conditions hold:

$$\begin{aligned}
i\omega g^{\varepsilon\pm} &= \frac{\partial P^\delta}{\partial n^\pm} \quad \text{on } \Gamma_\delta^\pm, \\
p^\varepsilon &= \hat{p}^\varepsilon = P^\delta \quad \text{on } \Gamma_\delta^\pm,
\end{aligned} \tag{10}$$

where n^\pm refers to normals \mathbf{n}^\pm outer to domains Ω_δ^\pm .

2.4. Plate model

The 3D model of an elastic plate involved in problem (1) can be replaced by a plate model which describes a thin structure. We assume a small $\varepsilon_0 > 0$

for which the limit model of acoustic transmission can be interpreted. In this paper we shall approximate behaviour of the thin elastic structure by the Reissner-Mindlin (R-M) plate model, which allows us to consider the effects related to shear stresses induced by rotations of the plate crosssections w.r.t. the mid-plane.

The R-M plate model can be obtained by the asymptotic analysis of the corresponding 3D elastic structure while its thickness $\tilde{h} \rightarrow 0$. However, the obtained limit model is then interpreted in terms of a given thickness $h > 0$. We shall discuss this point in Remark 1.

The plate is represented by its perforated mean surface Γ^ε , therefore all involved variables depend on ε . However, for a while we drop the superscript $^\varepsilon$ related to these variables. The plate deflections are described by amplitude of the membrane elastic wave $\mathbf{u} = (u_1, u_2)$, of the transverse wave u_3 and of the rotation wave $\boldsymbol{\theta} = (\theta_1, \theta_2)$. Two linear constitutive laws are involved, which depend upon the second order tensor $\mathbf{S} = (S_{ij}) = \varsigma \delta_{ij}$, where $\varsigma > 0$ is the shear coefficient, and the fourth order elasticity tensor $\mathbb{E} = (E_{ijkl})$ which is given by the Hooke law adapted for the plane stress constraint; we define (all indices $i, j, k, l = 1, 2$)

$$\begin{aligned} W_{ij}(\mathbf{v}) &:= E_{ijkl} \partial_l v_k = [\mathbb{E} \bar{\nabla}^S \mathbf{v}]_{ij}, \\ Z_i(u_3, \boldsymbol{\theta}) &:= S_{ij} (\partial_j u_3 - \theta_j) = [\mathbf{S} (\bar{\nabla} u_3 - \boldsymbol{\theta})]_i. \end{aligned} \tag{11}$$

The Reissner-Mindlin plate model is derived using the following kinematic ansatz confining the displacement $\mathbf{w} = (\bar{\mathbf{w}}, w_3)$ in a plate with the actual thickness h ,

$$\bar{\mathbf{w}}(x', z) = \bar{\mathbf{u}}(x') + h z \boldsymbol{\theta}(x'), \quad w_3(x', z) = u_3(x'), \quad z \in [-1, 1], \quad x' \in \Gamma^\varepsilon, \tag{12}$$

where $\bar{\mathbf{u}} = (u_1, u_2)$ is “membrane-mode” displacements, i.e. vector $\mathbf{u} = (\bar{\mathbf{u}}, u_3)$ involves also the “transversal mode” (the deflection). The vector

fields $(\mathbf{u}, \boldsymbol{\theta})$ satisfy the following equations in Γ^ε ,

$$\begin{aligned}
\omega^2 h \rho \bar{\mathbf{u}} + h \bar{\nabla} \cdot \mathbf{W}(\bar{\mathbf{u}}) &= -\bar{\mathbf{f}}(p), & \text{in } \Gamma^\varepsilon, \\
\omega^2 h \rho u_3 + h \bar{\nabla} \cdot \mathbf{Z}(u_3, \boldsymbol{\theta}) &= -f_3(p), & \text{in } \Gamma^\varepsilon, \\
\omega^2 \frac{h^3}{12} \rho \boldsymbol{\theta} + \frac{h^3}{12} \bar{\nabla} \cdot \mathbf{W}(\boldsymbol{\theta}) &= -\bar{\mathbf{m}}, & \text{in } \Gamma^\varepsilon, \\
h \bar{\mathbf{n}} \cdot \mathbf{W}(\bar{\mathbf{u}}) &= \bar{\mathbf{f}}^\partial & \text{on } \partial_o \Gamma^\varepsilon, \\
h \bar{\mathbf{n}} \cdot \mathbf{Z}(u_3, \boldsymbol{\theta}) &= f_3^\partial & \text{on } \partial_o \Gamma^\varepsilon, \\
\frac{h^3}{12} \bar{\mathbf{n}} \cdot \mathbf{W}(\boldsymbol{\theta}) &= \bar{\mathbf{m}}^\partial & \text{on } \partial_o \Gamma^\varepsilon, \\
\mathbf{u} &= 0 & \text{on } \partial_{\text{ext}} \Gamma^\varepsilon, \\
\boldsymbol{\theta} &= 0 & \text{on } \partial_{\text{ext}} \Gamma^\varepsilon,
\end{aligned} \tag{13}$$

where $\partial_o \Gamma^\varepsilon = \partial \Gamma^\varepsilon \setminus \partial_{\text{ext}} \Gamma^\varepsilon$ describes the perforations. Above the applied forces $\mathbf{f} = (\bar{\mathbf{f}}, f_3), \bar{\mathbf{f}}^\partial$ and moments $\bar{\mathbf{m}}, \bar{\mathbf{m}}^\partial$ depend on the acoustic potential p . The crucial step in deriving the model of vibroacoustic transmission consists in describing these forces in terms of p imposed on surface $\partial \Sigma^\varepsilon$ in the 3D plate representation.

Remark 1. In our asymptotic analysis of the acoustic transmission layer, we shall use the plate thickness in two contexts:

- The periodically perforated plate model defined in terms of the 2D domain $\Gamma^\varepsilon \subset \Gamma_0$ representing the mid-plane and the thickness $h = \varepsilon_0 \bar{h}$ with $\varepsilon_0 > 0$ being fixed. In fact, for a given thickness h and the perforation design (a given size of the holes yielding ε_0) we can obtain \bar{h} .
- To describe the interaction between the 3D elastic structure and the acoustic fluid, the thickness must be proportional to ε which is also related to the transmission layer thickness $\delta = \varkappa \varepsilon$, thus, we consider $h^\varepsilon = \varepsilon \bar{h}$ and the elastic body occupying domain Σ^ε , see (3).

Thus, the homogenization of the periodically perforated plate is done by pursuing the asymptotic analysis $\varepsilon \rightarrow 0$ applied to the 2D plate model (13) divided by h . Whereas h is fixed in the plate equation operator, being independent of ε , at the r.h.s. terms we get $1/(\varepsilon \bar{h})$ which is coherent with the dilation operation applied when dealing with fluid equation, see Section 2.7.

△

2.5. Variational formulation of the vibroacoustic problem in the layer

In order to derive the homogenized model of the transmission layer, we shall need the variational formulation of problem (9) with the plate model (13).

Find $p^\varepsilon \in H^1(\Omega^{*\varepsilon})$ and $(\mathbf{u}^\varepsilon, \boldsymbol{\theta}^\varepsilon) \in (H_0^1(\Omega))^5$ such that

$$c^2 \int_{\Omega^{*\varepsilon}} \nabla p^\varepsilon \cdot \nabla q^\varepsilon - \omega^2 \int_{\Omega^{*\varepsilon}} p^\varepsilon q^\varepsilon = -i\omega c^2 \left(\int_{\Gamma^{\pm\varepsilon}} g^{\varepsilon\pm} q^\varepsilon d\Gamma + \int_{\partial\Sigma^\varepsilon} \mathbf{n} \cdot \mathbf{w}^\varepsilon q^\varepsilon d\Gamma \right), \quad (14)$$

for all $q \in H^1(\Omega^{*\varepsilon})$, where \mathbf{n} is outward normal to domain Σ^ε , and

$$\begin{aligned} & \omega^2 h \int_{\Gamma^\varepsilon} \rho \mathbf{u}^\varepsilon \cdot \mathbf{v}^\varepsilon \omega^2 \frac{h^3}{12} \int_{\Gamma^\varepsilon} \rho \boldsymbol{\theta}^\varepsilon \cdot \boldsymbol{\psi}^\varepsilon - h \int_{\Gamma^\varepsilon} [\mathbb{E}^\varepsilon \bar{\nabla}^S \bar{\mathbf{u}}^\varepsilon] : \bar{\nabla}^S \bar{\mathbf{v}}^\varepsilon \\ & - h \int_{\Gamma^\varepsilon} [\mathbf{S}^\varepsilon (\bar{\nabla} u_3^\varepsilon - \theta^\varepsilon)] \cdot (\bar{\nabla} v_3^\varepsilon - \psi^\varepsilon) - \frac{h^3}{12} \int_{\Gamma^\varepsilon} [\mathbb{E}^\varepsilon \bar{\nabla}^S \boldsymbol{\theta}^\varepsilon] : \bar{\nabla}^S \boldsymbol{\psi}^\varepsilon \\ & = \int_{\Gamma^\varepsilon} \mathbf{f}^\varepsilon(p^\varepsilon) \cdot \mathbf{v}^\varepsilon + \int_{\Gamma^\varepsilon} \bar{\mathbf{m}}^\varepsilon(p^\varepsilon) \cdot \boldsymbol{\psi}^\varepsilon + \int_{\partial_o \Gamma^\varepsilon} \bar{\mathbf{f}}^{\partial,\varepsilon}(p^\varepsilon) \cdot \bar{\mathbf{v}}^\varepsilon + \int_{\partial_o \Gamma^\varepsilon} \bar{\mathbf{m}}^{\partial,\varepsilon}(p^\varepsilon) \cdot \boldsymbol{\psi}^\varepsilon, \end{aligned} \quad (15)$$

for all test functions $(\mathbf{v}^\varepsilon, \boldsymbol{\psi}^\varepsilon) \in (H_0^1(\Omega))^5$. In (14), the displacements \mathbf{w}^ε defined on the surface $\partial\Sigma^\varepsilon$ are expressed using the mid-plane kinematic fields. Due to (12), it holds that

$$\begin{aligned} \mathbf{w}^\varepsilon(x', x_3) &= (w_k^\varepsilon(x', x_3)), \\ w_\alpha^\varepsilon(x', x_3) &= u_\alpha^\varepsilon(x') - x_3 \theta_\alpha^\varepsilon(x'), \quad \alpha = 1, 2, \\ w_3^\varepsilon(x', x_3) &= u_3^\varepsilon(x'), \end{aligned} \quad (16)$$

where $x' \in \Gamma^\varepsilon$, $x_3 \in \varepsilon\bar{h}] - 1/2, 1/2[$. In analogy, the test displacements $\tilde{w}_k^\varepsilon(x', x_3)$ $k = 1, 2, 3$ can be introduced in terms of the test functions $(\mathbf{v}^\varepsilon, \boldsymbol{\psi}^\varepsilon)$ involved in (15); in this equation, the r.h.s. integrals express the virtual power

$$\int_{\partial_* \Sigma^\varepsilon} \mathbf{b}^\varepsilon \cdot \tilde{\mathbf{w}}^\varepsilon, \quad (17)$$

where the traction stress $\mathbf{b}^\varepsilon = i\omega\rho_0 \mathbf{n} p^\varepsilon$ is induced by the acoustic pressure in the fluid.

2.6. Fluid structure interaction on the plate surface $\partial\Sigma$

The forces and moments involved in the r.h.s. of (15) can be identified using the 3D representation of the plate surface $\partial_* \Sigma^\varepsilon$ decomposed according to (3). The actual surface traction $b_i^\varepsilon = i\omega\rho_0 n_i p^\varepsilon$ is given by the acoustic

potential and by the surface normal $\mathbf{n} = (n_i)$; note that $n_\alpha = 0$, $\alpha = 1, 2$ on $\partial_\pm \Sigma^\varepsilon$, whereas $n_3 = 0$ on $\partial_o \Sigma^\varepsilon$. Hence, it can be shown that the following expressions hold:

$$\begin{aligned} \bar{f}_\alpha^\varepsilon &= 0, \quad \bar{m}_\alpha^\varepsilon = 0, \quad f_3^\partial = 0, \\ \bar{f}_3^\varepsilon &= \sum_{s=+,-} b_3(x', s\varepsilon\bar{h}/2) = i\omega\rho_0(p^\varepsilon(x', \varepsilon\bar{h}/2) - p^\varepsilon(x', -\varepsilon\bar{h}/2)), \\ f_\alpha^{\partial,\varepsilon} &= \int_{-h^\varepsilon/2}^{h^\varepsilon/2} b_\alpha(x', x_3) dx_3 = i\omega\rho_0 \int_{-h^\varepsilon/2}^{h^\varepsilon/2} n_\alpha(x') p^\varepsilon(x', x_3) dx_3, \\ m_\alpha^{\partial,\varepsilon} &= - \int_{-h^\varepsilon/2}^{h^\varepsilon/2} x_3 b_\alpha(x', x_3) dx_3 = -i\omega\rho_0 \int_{-h^\varepsilon/2}^{h^\varepsilon/2} x_3 n_\alpha(x') p^\varepsilon(x', x_3) dx_3. \end{aligned} \tag{18}$$

Then we consider the fluid equation. In (14), in the integral on $\partial\Sigma^\varepsilon$, the displacement field \mathbf{w} must be expressed in terms of the mid-plane displacements and rotations \mathbf{u}^ε and $\boldsymbol{\theta}^\varepsilon$, as introduced in (16). This yields

$$\int_{\partial\Sigma^\varepsilon} \mathbf{n} \cdot \mathbf{w}^\varepsilon q^\varepsilon = \int_{\Gamma^\varepsilon} u_3^\varepsilon \llbracket q^\varepsilon(\cdot, x_3) \rrbracket_{\varepsilon\bar{h}}^\pm + \int_{\partial\Gamma^\varepsilon} \varepsilon\bar{h} \int_{-1/2}^{1/2} \bar{\mathbf{n}} \cdot (\mathbf{u}^\varepsilon - \varepsilon\bar{h}\zeta\boldsymbol{\theta}^\varepsilon) q^\varepsilon(\cdot, \varepsilon\bar{h}\zeta) d\zeta. \tag{19}$$

2.7. Dilated formulation

We can now state the vibro-acoustic problem in the dilated layer $\hat{\Omega} = \Gamma_0 \times]-\varkappa/2, +\varkappa/2[$, where the fluid occupies domain $\hat{\Omega}^* = \{(x', \varepsilon^{-1}x_3) \in \mathbb{R}^3 | x \in \Omega^{*\varepsilon}\}$, see (6). Using $z = \varepsilon^{-1}x_3$, while $x' = (x_\alpha)$, with new coordinates (x', z) , the gradients are $\hat{\nabla} = (\partial_\alpha, \varepsilon^{-1}\partial_z)$, thus $\nabla p(x) = \hat{\nabla} p(x_\alpha, z)$; to simplify the notation, we shall use the same notation for functions depending on x_3 , but expressed in terms of z .

By virtue of the dilation and the periodic unfolding, the vibroacoustic problem can be transformed in the domain which does not change with ε . Consequently the standard means of convergence can be used to obtain the limit model.

Equation (14) with the substitution (19) can now be transformed by the dilatation (the same notation for all variables is adhered, but should be interpreted in this new context of this dilated formulation):

$$\begin{aligned} & \int_{\hat{\Omega}^\varepsilon} \hat{\nabla} p^\varepsilon \cdot \hat{\nabla} q^\varepsilon - \frac{\omega^2}{c^2} \int_{\hat{\Omega}^\varepsilon} p^\varepsilon q^\varepsilon = -\frac{i\omega}{\varepsilon} \int_{\Gamma^\pm} \hat{g}^{\varepsilon\pm} q^\varepsilon \\ & - \frac{i\omega}{\varepsilon} \left[\int_{\Gamma^\varepsilon} u_3^\varepsilon \llbracket q^\varepsilon(\cdot, x_3) \rrbracket_{\varepsilon\bar{h}}^\pm + \int_{\partial_o \Gamma^\varepsilon} \varepsilon\bar{h} \int_{-1/2}^{1/2} \bar{\mathbf{n}} \cdot (\bar{\mathbf{u}}^\varepsilon - \varepsilon\bar{h}\zeta\boldsymbol{\theta}^\varepsilon) q^\varepsilon(\cdot, \varepsilon\bar{h}\zeta) d\zeta \right]. \end{aligned} \tag{20}$$

Further we employ (18) to rewrite (15) which is divided by h^ε ; by virtue of Remark 1, the plate thickness is given, *i.e.* $h = \varepsilon_0 \bar{h}$, however, when dealing with the r.h.s. interaction terms, $h := h^\varepsilon = \varepsilon \bar{h}$ in accordance with the dilation transformation. Thus we get

$$\begin{aligned} & \omega^2 \int_{\Gamma^\varepsilon} \rho \mathbf{u}^\varepsilon \cdot \mathbf{v}^\varepsilon + \omega^2 \frac{h^2}{12} \int_{\Gamma^\varepsilon} \rho \boldsymbol{\theta}^\varepsilon \cdot \boldsymbol{\psi}^\varepsilon \\ & - \int_{\Gamma^\varepsilon} [\mathbb{E}^\varepsilon \bar{\nabla}^S \bar{\mathbf{u}}^\varepsilon] : \bar{\nabla}^S \bar{\mathbf{v}}^\varepsilon - \int_{\Gamma^\varepsilon} [\mathbf{S}^\varepsilon (\bar{\nabla} u_3^\varepsilon - \boldsymbol{\theta}^\varepsilon)] \cdot (\bar{\nabla} v_3^\varepsilon - \boldsymbol{\psi}^\varepsilon) - \frac{h^2}{12} \int_{\Gamma^\varepsilon} [\mathbb{E}^\varepsilon \bar{\nabla}^S \boldsymbol{\theta}^\varepsilon] : \bar{\nabla}^S \boldsymbol{\psi}^\varepsilon \\ & = \frac{i\omega\rho_0}{\varepsilon\bar{h}} \left[\int_{\Gamma^\varepsilon} v_3^\varepsilon \llbracket p^\varepsilon(\cdot, x_3) \rrbracket_{\varepsilon\bar{h}}^\pm + \varepsilon\bar{h} \int_{\partial_0\Gamma^\varepsilon} \int_{-1/2}^{1/2} p^\varepsilon(\cdot, \varepsilon\bar{h}\zeta) \bar{\mathbf{n}} \cdot (\bar{\mathbf{v}}^\varepsilon - \varepsilon\bar{h}\zeta \boldsymbol{\psi}^\varepsilon) d\zeta \right]. \end{aligned} \quad (21)$$

It is worth noting that, in (20) and (21), the r.h.s. integrals provide a symmetry of the following formulation.

The problem formulation. The vibroacoustic interaction in the dilated layer $\hat{\Omega}_\delta$ is described by $(p^\varepsilon, \mathbf{u}^\varepsilon, \boldsymbol{\theta}^\varepsilon) \in H^1(\hat{\Omega}^{*\varepsilon}) \times (H_0^1(\Gamma^\varepsilon))^5$ which satisfy equations (20)-(21) for any test fields $(q^\varepsilon, \mathbf{v}^\varepsilon, \boldsymbol{\psi}^\varepsilon) \in H^1(\hat{\Omega}^{*\varepsilon}) \times (H_0^1(\Gamma^\varepsilon))^5$.

Let $g^0 \in L^2(\Gamma_0)$ and $g^{1\pm}(x', y') \in L^2(\Gamma_0 \times \mathbb{R}^2)$, whereby $g^{1\pm}(x', \cdot)$ being Ξ -periodic in the second variable; we define

$$\begin{aligned} \hat{g}^{\varepsilon+}(x') &= g^0(x') + \varepsilon g^{1+}(x', \frac{x'}{\varepsilon}), \\ \hat{g}^{\varepsilon-}(x') &= -g^0(x') - \varepsilon g^{1-}(x', \frac{x'}{\varepsilon}). \end{aligned} \quad (22)$$

For any $\varepsilon > 0$ and $\hat{g}^{\varepsilon\pm}$ defined according to (22), the vibroacoustic interaction problem constituted by equations (20)-(21) possesses a unique solution $(p^\varepsilon, \mathbf{u}^\varepsilon, \boldsymbol{\theta}^\varepsilon)$. As an essential step of the proof, the *a priori* estimates are derived in the Appendix A.1.

3. Homogenization of the transmission layer

In this section, we introduce the convergence result which yields the limit acoustic pressure and the plate displacements and rotations. These are involved in the limit two-scale equations of the vibroacoustic problem imposed in the transmission layer. The asymptotic analysis is based on the unfolding method which was inaugurated in the seminal paper [4] and elaborated further for thin structures in [3]. In our setting, the unfolding operator $\mathcal{T}_\varepsilon : L^2(\Omega_\delta; \mathbb{R}) \rightarrow L^2(\Gamma_0 \times Y; \mathbb{R})$ transforms a function $f(x)$ defined in Ω_δ into a function of two variables, $x' \in \Gamma_0$ and $y \in Y$. For any $f \in L^1(Y)$, the

cell average involved in all unfolding intergartion formulae will be abbreviated by

$$\frac{1}{|\Xi|} \int_{\Xi} f = \oint_{\Xi} f \quad \frac{1}{|\Xi|} \int_D f =: \oint_D f , \quad (23)$$

whatever the domain $D \subset \overline{Y}$ of the the integral is (*i.e.* volume, or surface).

3.1. The convergence results

Based on the a priori estimates derived in the Appendix A, the following theorem holds.

Theorem 1. *Let us assume*

$$\begin{aligned} \|p^\varepsilon\|_{L^2(\hat{\Omega}^{*\varepsilon})} &\leq C , & \|\overline{\mathbf{u}}^\varepsilon\|_{[L^2(\Gamma^\varepsilon)]^2} &\leq C , \\ \|u_3^\varepsilon\|_{L^2(\Gamma^\varepsilon)} &\leq C , & \|\theta^\varepsilon\|_{[L^2(\Gamma^\varepsilon)]^2} &\leq C , \end{aligned} \quad (24)$$

then the following estimates can be obtained:

$$\begin{aligned} \|\hat{\nabla} p^\varepsilon\|_{[L^2(\hat{\Omega}^{*\varepsilon})]^3} &\leq C , & \|\overline{\nabla} \overline{\mathbf{u}}^\varepsilon\|_{[L^2(\Gamma^\varepsilon)]^4} &\leq C , \\ \|\overline{\nabla} u_3^\varepsilon\|_{[L^2(\Gamma^\varepsilon)]^2} &\leq C , & \|\overline{\nabla} \theta^\varepsilon\|_{[L^2(\Gamma^\varepsilon)]^4} &\leq C . \end{aligned} \quad (25)$$

Since $\hat{\nabla} p^\varepsilon = (\overline{\nabla} p^\varepsilon, \varepsilon^{-1} \partial_z p^\varepsilon)$, we have

$$\|\overline{\nabla} p^\varepsilon\|_{[L^2(\hat{\Omega}^{*\varepsilon})]^2} \leq C , \quad \|\partial_z p^\varepsilon\|_{[L^2(\hat{\Omega}^{*\varepsilon})]^2} \leq \varepsilon C . \quad (26)$$

Due to Theorem 1 providing the estimates (24)-(26) we obtain the convergence of the unfolded functions (For the definition of the unfolding operator we refere *e.g.* to [4]). First we observe (note (26)₂):

$$\begin{aligned} p^\varepsilon &\rightharpoonup p^0 \quad \text{w. in } L^2(\hat{\Omega}) , \\ \partial_z p^\varepsilon &\rightharpoonup 0 \quad \text{w. in } L^2(\hat{\Omega}) , \end{aligned} \quad (27)$$

thus, $\partial_z p^0 = 0$. The classical results of the unfolding method of homogenization yield

$$\begin{aligned} \mathcal{T}_\varepsilon(p^\varepsilon) &\rightharpoonup p^0 \quad \text{w. in } L^2(\Gamma_0 \times Y^*) , \\ \mathcal{T}_\varepsilon(\overline{\nabla} p^\varepsilon) &\rightharpoonup \overline{\nabla}_x p^0 + \overline{\nabla}_y p^1 \quad \text{w. in } L^2(\Gamma_0 \times Y^*) , \\ \frac{1}{\varepsilon} \mathcal{T}_\varepsilon(\partial_z p^\varepsilon) &\rightharpoonup \partial_z p^1 \quad \text{w. in } L^2(\Gamma_0 \times Y^*) . \end{aligned} \quad (28)$$

Above $p^0 \in H^1(\Gamma_0)$ and $p^1 \in L^2(\Gamma_0; H_{\#}^1(Y^*))$, where $H_{\#}^1(Y^*)$ is the subspace of $H^1(Y)$ generated by Ξ -periodic functions (thus, the periodicity in y_α holds, but not in $y_3 = z$), with vanishing average in Y .

For the plate responses we get

$$\begin{aligned} \mathbf{u}^\varepsilon &\rightharpoonup \mathbf{u}^0 \quad \text{s. in } [L^2(\Gamma_K)]^2, \\ \mathcal{T}_\varepsilon(\mathbf{u}^\varepsilon) &\rightharpoonup \mathbf{u}^0 \quad \text{w. in } [L^2(\Gamma_K \times \Xi_K)]^3, \\ \mathcal{T}_\varepsilon(\nabla \mathbf{u}^\varepsilon) &\rightharpoonup \nabla_{x'} \mathbf{u}^0 + \nabla_{y'} \mathbf{u}^1 \quad \text{w. in } [L^2(\Gamma_0 \times \Xi_S)]^6, \end{aligned} \quad (29)$$

where $\mathbf{u}^0 \in [H^1(\Gamma_K)]^3$ and $\mathbf{u}^1 \in L^2(\Gamma_K; [H_{\#}^1(\Xi_K)]^3)$. Here $H_{\#}^1(\Xi_K)$ is subspace of $H^1(\Xi)$ involving only Ξ -periodic functions with vanishing average in Ξ_K . For the rotations we obtain

$$\begin{aligned} \mathcal{T}_\varepsilon(\boldsymbol{\theta}^\varepsilon) &\rightharpoonup \boldsymbol{\theta}^0 \quad \text{w. in } [L^2(\Gamma_0 \times \Xi_S)]^2, \\ \mathcal{T}_\varepsilon(\nabla \boldsymbol{\theta}^\varepsilon) &\rightharpoonup \nabla_{x'} \boldsymbol{\theta}^0 + \nabla_{y'} \boldsymbol{\theta}^1 \quad \text{w. in } [L^2(\Gamma_0 \times \Xi)]^4, \end{aligned} \quad (30)$$

where $\boldsymbol{\theta}^0 \in [H^1(\Gamma_K)]^2$ and $\boldsymbol{\theta}^1 \in L^2(\Gamma_0; [H_{\#}^1(\Xi_S)]^2)$.

The limit vibro-acoustic problem can be derived by a formal approach which relies on the recovery sequences (w.r.t. ε) constructed in accordance with the convergence result. Neglecting the higher order terms in ε , the following approximate expansions for unfolded vibroacoustic fields ($p^\varepsilon, \mathbf{u}^\varepsilon, \boldsymbol{\theta}^\varepsilon$) are considered:

$$\begin{aligned} \mathcal{T}_\varepsilon(p^\varepsilon) &= p^0(x') + \varepsilon p^1(x', y), \\ \mathcal{T}_\varepsilon(\bar{\mathbf{u}}^\varepsilon) &= \bar{\mathbf{u}}^0(x') + \varepsilon \bar{\mathbf{u}}^1(x', y'), \\ \mathcal{T}_\varepsilon(u_3^\varepsilon) &= u_3^0(x') + \varepsilon u_3^1(x', y'), \\ \mathcal{T}_\varepsilon(\boldsymbol{\theta}^\varepsilon) &= \boldsymbol{\theta}^0(x') + \varepsilon \boldsymbol{\theta}^1(x', y'), \end{aligned} \quad (31)$$

where $x' \in \Gamma_0$, $y' \in \Xi$ and $y = (y', z) \in Y$; in (31), all the two-scale functions are Ξ -periodic in the second variable. Analogous expansions involving two-scale functions periodic in y' will be employed as the test functions involved in (20)-(21),

$$\begin{aligned} \mathcal{T}_\varepsilon(q^\varepsilon) &= q^0(x') + \varepsilon q^1(x', y), \\ \mathcal{T}_\varepsilon(\bar{\mathbf{v}}^\varepsilon) &= \bar{\mathbf{v}}^0(x') + \varepsilon \bar{\mathbf{v}}^1(x', y'), \\ \mathcal{T}_\varepsilon(v_3^\varepsilon) &= v_3^0(x') + \varepsilon v_3^1(x', y'), \\ \mathcal{T}_\varepsilon(\boldsymbol{\psi}^\varepsilon) &= \boldsymbol{\psi}^0(x') + \varepsilon \boldsymbol{\psi}^1(x', y'). \end{aligned} \quad (32)$$

It is worth to note that the use of the recovery sequences simplifies the derivation of limit equations of the vibro-acoustic model which, however, can be obtained more rigorously using the asymptotic analysis applied directly to equations (20)-(21). We shall substitute the ansatz (31)-(32) in unfolded equations (20)-(21) and explore the limit form for $\varepsilon \rightarrow 0$.

3.2. Limit fluid equation

The unfolded left hand side of (20) yields the following limit form:

$$\begin{aligned} & c^2 \int_{\Gamma_0} \oint_{Y^*} \mathcal{T}_\varepsilon(\bar{\nabla} p^\varepsilon) \cdot \mathcal{T}_\varepsilon(\bar{\nabla} q^\varepsilon) + \frac{c^2}{\varepsilon^2} \int_{\Gamma_0} \oint_{Y^*} \partial_z \mathcal{T}_\varepsilon(p^\varepsilon) \partial_z \mathcal{T}_\varepsilon(q^\varepsilon) - \omega^2 \int_{\Gamma_0} \oint_{Y^*} \mathcal{T}_\varepsilon(p^\varepsilon) \mathcal{T}_\varepsilon(q^\varepsilon) \\ & \rightarrow c^2 \int_{\Gamma_0} \oint_{Y^*} (\bar{\nabla}_x p^0 + \bar{\nabla}_y p^1) \cdot (\bar{\nabla}_x q^0 + \bar{\nabla}_y q^1) + c^2 \int_{\Gamma_0} \oint_{Y^*} \partial_z p^1 \partial_z q^1 - \omega^2 \int_{\Gamma_0} \oint_{Y^*} p^0 q^0. \end{aligned} \quad (33)$$

The unfolded right hand side integrals can be written, as follows:

$$\begin{aligned} & -\frac{i\omega c^2}{\varepsilon} \int_{\Gamma_0} \left[\oint_{I_y^+} (g^0 + \varepsilon g^{1+})(q^0 + \varepsilon q^1) + \oint_{I_y^-} (-g^0 - \varepsilon g^{1-})(q^0 + \varepsilon q^1) \right] \\ & -\frac{i\omega c^2}{\varepsilon} \int_{\Gamma_0} \left[\oint_{\Xi_S} \mathcal{T}_\varepsilon(u_3^\varepsilon) [\varepsilon q^1(\cdot, z)]_h^\pm \right. \\ & \quad \left. + \frac{\varepsilon \bar{h}}{\varepsilon} \oint_{\partial \Xi_S} \int_{-1/2}^{1/2} \bar{\mathbf{n}} \cdot (\mathcal{T}_\varepsilon(\bar{\mathbf{u}}^\varepsilon) - \varepsilon \bar{h} \zeta \mathcal{T}_\varepsilon(\boldsymbol{\theta}^\varepsilon)) (q^0(x') + \varepsilon q^1(x', y', \bar{h} \zeta)) d\zeta \right]. \end{aligned} \quad (34)$$

In the limit, the first integral related to the dilated fictitious interfaces Γ^\pm yields

$$-i\omega c^2 \int_{\Gamma_0} \left(q^0 \oint_{\Xi} (g^{1+} - g^{1-}) + g^0 \left(\oint_{I_y^+} q^1 - \oint_{I_y^-} q^1 \right) \right). \quad (35)$$

The second integral in (34) can be rewritten, as follows (omitting the factor $-i\omega c^2$)

$$\begin{aligned} & \frac{1}{\varepsilon} \int_{\Gamma_0} \oint_{\Xi_S} (u_3^0 + \varepsilon u_3^1) \varepsilon [q^1]_h^\pm \\ & + \frac{\bar{h}}{\varepsilon} \int_{\Gamma_0} \oint_{\partial \Xi_S} \int_{-1/2}^{1/2} \bar{\mathbf{n}} \cdot (\bar{\mathbf{u}}^0 + \varepsilon \bar{\mathbf{u}}^1 - \varepsilon \bar{h} \zeta (\boldsymbol{\theta}^0 + \varepsilon \boldsymbol{\theta}^1)) (q^0 + \varepsilon q^1), \end{aligned} \quad (36)$$

where only $q^1(x', y', \bar{h} \zeta)$ depends on $\zeta \in]-1/2, +1/2[$. Hence, since $\int_{-1/2}^{1/2} \zeta = 0$, in the limit, the second integral in (34) yields

$$-i\omega c^2 \int_{\Gamma_0} \left(u_3^0 \oint_{\Xi_S} [q^1]_h^\pm + \bar{\mathbf{u}}^0 \cdot \oint_{\partial \Xi_S} \bar{\mathbf{n}} \bar{h} \int_{-1/2}^{1/2} q^1 d\zeta + q^0 \bar{h} \oint_{\partial \Xi_S} \bar{\mathbf{n}} \cdot \bar{\mathbf{u}}^1 \right). \quad (37)$$

Now the limit fluid equation constituted using (33)(35) and (37) attains the following form:

$$\begin{aligned}
& c^2 \int_{\Gamma_0} \oint_{Y^*} (\bar{\nabla}_x p^0 + \bar{\nabla}_y p^1) \cdot (\bar{\nabla}_x q^0 + \bar{\nabla}_y q^1) + c^2 \int_{\Gamma_0} \oint_{Y^*} \partial_z p^1 \partial_z q^1 - \omega^2 \int_{\Gamma_0} \oint_{Y^*} p^0 q^0 \\
& = -i\omega c^2 \int_{\Gamma_0} \left[q^0 \oint_{\Xi} \Delta g^1 + g^0 \left(\oint_{I_y^+} q^1 - \oint_{I_y^-} q^1 \right) \right. \\
& \left. + u_3^0 \oint_{\Xi_S} \llbracket q^1 \rrbracket_h^\pm + \bar{\mathbf{u}}^0 \cdot \oint_{\partial \Xi_S} \bar{\mathbf{n}} \bar{h} \int_{-1/2}^{1/2} q^1 d\zeta + q^0 \bar{h} \oint_{\partial \Xi_S} \bar{\mathbf{n}} \cdot \bar{\mathbf{u}}^1 \right]
\end{aligned} \tag{38}$$

where $\Delta g^1 = g^{1+} - g^{1-}$.

3.3. Limit plate equation

The unfolded left hand side of (21) yields the following limit form:

$$\begin{aligned}
& -\omega^2 \int_{\Gamma_0} \rho_S \left(\mathbf{u}^0 \cdot \mathbf{v}^0 + \frac{h^2}{12} \boldsymbol{\theta}^0 \cdot \boldsymbol{\psi}^0 \right) + \int_{\Gamma_0} \oint_{\Xi_S} [\mathbb{E}(\bar{\nabla}_x^S \bar{\mathbf{u}}^0 + \bar{\nabla}_y^S \bar{\mathbf{u}}^1)] : (\bar{\nabla}_x^S \bar{\mathbf{v}}^0 + \bar{\nabla}_y^S \bar{\mathbf{v}}^1) \\
& \quad + \int_{\Gamma_0} \oint_{\Xi_S} \mathbf{S}(\bar{\nabla}_x u_3^0 + \bar{\nabla}_y u_3^1 - \boldsymbol{\theta}^0) \cdot (\bar{\nabla}_x v_3^0 + \bar{\nabla}_y v_3^1 - \boldsymbol{\psi}^0) \\
& \quad + \frac{h^2}{12} \int_{\Gamma_0} \oint_{\Xi_S} [\mathbb{E}(\bar{\nabla}_x^S \boldsymbol{\theta}^0 + \bar{\nabla}_y^S \boldsymbol{\theta}^1)] : (\bar{\nabla}_x^S \boldsymbol{\psi}^0 + \bar{\nabla}_y^S \boldsymbol{\psi}^1)
\end{aligned} \tag{39}$$

The unfolded right hand side integrals can be written in analogy with the ones involved in the fluid equation, see (36). Since the role of the solution and the test function switches, the unfolded form of (21) yields

$$\begin{aligned}
& \frac{i\omega\rho_0}{\varepsilon\bar{h}} \int_{\Gamma_0} \oint_{\Xi_S} (v_3^0 + \varepsilon v_3^1) \varepsilon \llbracket p^1 \rrbracket_h^\pm \\
& + \frac{i\omega\rho_0}{\varepsilon} \int_{\Gamma_0} \oint_{\partial \Xi_S} \int_{-1/2}^{1/2} \bar{\mathbf{n}} \cdot (\bar{\mathbf{v}}^0 + \varepsilon \bar{\mathbf{v}}^1 - \varepsilon \bar{h} \zeta (\boldsymbol{\psi}^0 + \varepsilon \boldsymbol{\psi}^1)) (p^0 + \varepsilon p^1) ,
\end{aligned} \tag{40}$$

which, in the limit, yields an analogous expression as the one of (37). Thus, the limit of the plate equation (21) is constituted by (39) which equals to

$$(39) = i\omega\rho_0 \int_{\Gamma_0} \left(v_3^0 \frac{1}{\bar{h}} \oint_{\Xi_S} \llbracket p^1 \rrbracket_h^\pm + \bar{\mathbf{v}}^0 \cdot \oint_{\partial \Xi_S} \bar{\mathbf{n}} \int_{-1/2}^{1/2} p^1 d\zeta + p^0 \oint_{\partial \Xi_S} \bar{\mathbf{n}} \cdot \bar{\mathbf{v}}^1 \right) . \tag{41}$$

Remark 2. Integrals over the plate surface involving q^1 and p^1 in (37) and (41), respectively, can be written in a more compact form; for any two-scale function $\varphi(x', y', \zeta)$ it holds that

$$v_3^0 \frac{1}{h} \oint_{\Xi_S} [\![\varphi]\!]_h^\pm dy' + \bar{\mathbf{v}}^0 \cdot \oint_{\partial \Xi_S} \bar{\mathbf{n}} \int_{-1/2}^{1/2} \varphi d\zeta = \frac{1}{h} \bar{\mathbf{v}}^0 \cdot \oint_{\partial S} \mathbf{n} \varphi . \quad (42)$$

△

3.4. Local problems in Y^*

When testing the limit equation (38) with $q^1 \neq 0$ while $q^0 = 0$, the local problem in the fluid part is obtained which reveals linear dependence of p^1 on the “macroscopic” functions \mathbf{u}^0, p^0 and g^0 . Therefore, we can introduce the following split:

$$p^1(x', y) = \pi^\beta(y) \partial_\beta^x p^0(x') + i\omega \xi(y) g^0(x') + i\omega \eta^k(y) u_k^0(x') , \quad (43)$$

where $y = (y', z) \in Y^*$, and introduce the following 3 autonomous problems for $\pi^\beta, \xi, \eta^k \in H_\#^1(Y^*)$:

$$\begin{aligned} (\nabla_y \pi^\beta, \nabla_y \psi)_{Y^*} &= - \int_{Y^*} \partial_\beta^y \psi , \quad \forall \psi \in H_\#^1(Y^*) , \quad \beta = 1, 2 , \\ (\nabla_y \xi, \nabla_y \psi)_{Y^*} &= - \left(\int_{I_y^+} \psi - \int_{I_y^-} \psi \right) , \quad \forall \psi \in H_\#^1(Y^*) , \\ (\nabla_y \eta^k, \nabla_y \psi)_{Y^*} &= - \int_{\partial S} n_k \psi \quad \forall \psi \in H_\#^1(Y^*) , \quad k = 1, 2, 3 . \end{aligned} \quad (44)$$

3.5. Local problems on Ξ_S

We consider the limit equation governing the plate response; its left and right hand sides are constituted by (39) and (41), respectively. Upon testing there subsequently by $\boldsymbol{\psi}^1, \bar{\mathbf{v}}^1$ and v_3^1 , whereas all $\boldsymbol{\psi}^0, \bar{\mathbf{v}}^0$ and v_3^0 vanish, the following local “microscopic” equations are obtained,

$$\begin{aligned} \frac{h^2}{12} \int_{\Gamma_0} \oint_{\Xi_S} [\mathbb{E}(\bar{\nabla}_x^S \boldsymbol{\theta}^0 + \bar{\nabla}_y^S \boldsymbol{\theta}^1)] : \bar{\nabla}_y^S \boldsymbol{\psi}^1 &= 0 , \quad \forall \boldsymbol{\psi}^1 \in L^2(\Gamma_0; (H_\#^1(\Xi_S))^2) , \\ \int_{\Gamma_0} \oint_{\Xi_S} \mathbb{E}(\bar{\nabla}_x^S \bar{\mathbf{u}}^0 + \bar{\nabla}_y^S \bar{\mathbf{u}}^1) : \bar{\nabla}_y^S \bar{\mathbf{v}}^1 &= i\omega \rho_0 \int_{\Gamma_0} p^0 \oint_{\partial \Xi_S} \bar{\mathbf{n}} \cdot \bar{\mathbf{v}}^1 , \quad \forall \bar{\mathbf{v}}^1 \in L^2(\Gamma_0; (H_\#^1(\Xi_S))^2) , \\ \int_{\Gamma_0} \oint_{\Xi_S} \mathbf{S}(\bar{\nabla}_x u_3^0 + \bar{\nabla}_y u_3^1 - \boldsymbol{\theta}^0) \cdot \bar{\nabla}_y v_3^1 &= 0 , \quad \forall v_3^1 \in L^2(\Gamma_0; H_\#^1(\Xi_S)) . \end{aligned} \quad (45)$$

Due to the linearity of (45), the following split of the two-scale functions can be introduced

$$\bar{\mathbf{u}}^1 = \bar{\chi}^{\alpha\beta}(\bar{\nabla}^S \bar{\mathbf{u}}^0)_{\alpha\beta} + \bar{\chi}^* i\omega \rho_0 p^0, \quad (46)$$

$$u_3^1 = \chi^k ((\bar{\nabla} u_3)_k - \theta_k), \quad (47)$$

$$\boldsymbol{\theta}^1 = \bar{\chi}^{\alpha\beta}(\bar{\nabla}^S \boldsymbol{\theta}^0)_{\alpha\beta}, \quad (48)$$

where $\bar{\chi}^{\alpha\beta}, \bar{\chi}^* \in \mathbf{H}_{\#}^1(\Xi_S)$, and $\chi^k \in H_{\#}^1(\Xi_S)$ are the corrector functions. They express the local characteristic responses of the plate which can be computed independently of the macroscopic responses $\bar{\nabla}^S \bar{\mathbf{u}}^0$, $\bar{\nabla}^S \boldsymbol{\theta}^0$, $\bar{\nabla} u_3$, and p^0 . It is worth noting that the same functions $\bar{\chi}^{\alpha\beta}$ are involved in both $\bar{\mathbf{u}}^1$ and $\boldsymbol{\theta}^1$ due to the similar structure of (45)₁ and (45)₂. The following three local autonomous problems have to be solved,

- Find $\bar{\chi}^{\alpha\beta} \in \mathbf{H}_{\#}^1(\Xi_S)/\mathbb{R}^2$ such that

$$\oint_{\Xi_S} (\mathbb{E} \bar{\nabla}_y^S (\bar{\chi}^{\alpha\beta} + \boldsymbol{\Pi}^{\alpha\beta}) : \bar{\nabla}_y^S \bar{\mathbf{v}} = 0 \quad \forall \bar{\mathbf{v}} \in \mathbf{H}_{\#}^1(\Xi_S), \quad (49)$$

where $\boldsymbol{\Pi}^{\alpha\beta} = (\Pi_{\nu}^{\alpha\beta})$, $\Pi_{\nu}^{\alpha\beta} = y_{\beta} \delta_{\alpha i}$ with $\nu, \alpha, \beta = 1, 2$.

- Find $\chi^{\alpha} \in H_{\#}^1(\Xi_S)/\mathbb{R}$ such that

$$\oint_{\Xi_S} (\mathbf{S} \nabla_y (\chi^{\alpha} + y_{\alpha})) \cdot \nabla_y \tilde{z} = 0 \quad \forall \tilde{z} \in H_{\#}^1(\Xi_S), \quad \alpha = 1, 2. \quad (50)$$

- Find $\bar{\chi}^* \in \mathbf{H}_{\#}^1(\Xi_S)/\mathbb{R}^2$ such that

$$\oint_{\Xi_S} \mathbb{E} \bar{\nabla}_y^S \bar{\chi}^* : \bar{\nabla}_y^S \bar{\mathbf{v}} = \oint_{\partial \Xi_S} \bar{\mathbf{n}} \cdot \bar{\mathbf{v}}, \quad \forall \bar{\mathbf{v}} \in \mathbf{H}_{\#}^1(\Xi_S). \quad (51)$$

3.6. Homogenized equations associated with the fluid

The macroscopic equation governing the acoustic potential p^0 distributed on the homogenized interface Γ_0 is obtained upon testing (20) with $q^0 \neq 0$ while $q^1 = 0$, which yields

$$\begin{aligned} & c^2 \int_{\Gamma_0} \oint_{Y^*} (\bar{\nabla}_x p^0 + \bar{\nabla}_y p^1) \cdot \bar{\nabla}_x q^0 - \omega^2 \int_{\Gamma_0} \oint_{Y^*} p^0 q^0 \\ & = -i\omega c^2 \int_{\Gamma_0} q_0 \left(\oint_{\Xi} \Delta g^1 + \bar{h} \oint_{\partial \Xi_S} \bar{\mathbf{n}} \cdot \bar{\mathbf{u}}^1 \right), \end{aligned} \quad (52)$$

where Δg^1 was introduced in (38). By virtue of the multiplicative splits (43) and (46), the integrals over Y^* , Ξ_S and $\partial \Xi_S$ involving the two-scale

functions can be expressed in terms of the macroscopic variables and using the homogenized coefficients $\mathbf{A} = (A_{\alpha\beta})$, $\mathbf{B} = (B_\alpha)$, $\mathbf{D} = (D_k)$, $\mathbf{H} = (H_{\alpha\beta})$ and K ,

$$\begin{aligned}
A_{\alpha\beta} &= \oint_{Y^*} \nabla_y(\pi^\beta + y_\beta) \cdot \nabla_y(\pi^\alpha + y_\alpha) , \\
B_\alpha &= \oint_{Y^*} \partial_\alpha^y \xi , \\
D_k^\alpha &= \oint_{Y^*} \partial_\alpha^y \eta^k = \int_{\partial S} n_k \pi^\alpha , \\
H_{\alpha\beta} &= \oint_{\partial \Xi_S} \bar{\mathbf{n}} \cdot \bar{\chi}^{\alpha\beta} , \\
K &= \oint_{\partial \Xi_S} \bar{\mathbf{n}} \cdot \bar{\chi}^* .
\end{aligned} \tag{53}$$

The alternative expression of P_k^α by π^α is obtained due to the local problems (44).

Finally we can obtain the following *extended equations of the acoustic transmission* satisfied by $(p^0, g^0) \in H^1(\Gamma_0) \times L^2(\Gamma_0)$

$$\begin{aligned}
& c^2 \int_{\Gamma_0} (\mathbf{A} \bar{\nabla}_x p^0) \cdot \bar{\nabla}_x q^0 - \zeta^* \omega^2 \int_{\Gamma_0} p^0 q^0 + i\omega c^2 \int_{\Gamma_0} g^0 \mathbf{B} \cdot \bar{\nabla}_x q^0 + i\omega c^2 \int_{\Gamma_0} \bar{\nabla}_x q^0 \cdot \mathbf{D} \mathbf{u}^0 \\
&= -i\omega c^2 \bar{h} \int_{\Gamma_0} q^0 \left(\frac{1}{\bar{h}} \oint_{\Xi} \Delta g^1 + i\omega \rho_0 K p^0 + \mathbf{H} : \bar{\nabla}_x^S \bar{\mathbf{u}}^0 \right) ,
\end{aligned} \tag{54}$$

for all $q^0 \in H^1(\Gamma_0)$, where $\zeta^* = |Y^*|/|\Xi|$.

3.7. Homogenized equations associated with the plate

In the limit equation governing the plate response, see (39) and (41), we apply the macroscopic test functions $\mathbf{v}^0, \boldsymbol{\psi}^0$, whereas we put $\mathbf{v}^1 = 0$ and $\boldsymbol{\vartheta}^1 = 0$. Thus we obtain

$$\begin{aligned}
& -\omega^2 \left(\int_{\Gamma_0} \oint_{\Xi_S} \rho_S \mathbf{u}^0 \cdot \mathbf{v}^0 + \frac{h^2}{12} \int_{\Gamma_0} \oint_{\Xi_S} \rho_S \boldsymbol{\theta}^0 \cdot \boldsymbol{\vartheta}^0 \right) \\
& + \int_{\Gamma_0} \oint_{\Xi_S} (\mathbf{S}(\bar{\nabla}_y u_3^1 + \bar{\nabla}_x u_3^0 - \boldsymbol{\theta}^0)) \cdot (\bar{\nabla}_x v_3^0 - \boldsymbol{\psi}^0) \\
& + \frac{h^2}{12} \int_{\Gamma_0} \oint_{\Xi_S} (\mathbb{E}(\bar{\nabla}_y^S \boldsymbol{\theta}^1 + \bar{\nabla}_x^S \boldsymbol{\theta}^0)) : \bar{\nabla}_x^S \boldsymbol{\psi}^0 + \int_{\Gamma_0} \oint_{\Xi_S} (\mathbb{E}(\bar{\nabla}_y^S \bar{\mathbf{u}}^1 + \bar{\nabla}_x^S \bar{\mathbf{u}}^0)) : \bar{\nabla}_x^S \bar{\mathbf{v}}^0 \\
& = i\omega \rho_0 \int_{\Gamma_0} \left(\mathbf{v}^3 \frac{1}{\bar{h}} \cdot \oint_{\partial S} \mathbf{n} p^1 \right) ,
\end{aligned} \tag{55}$$

Upon substituting (\mathbf{u}^1, θ^1) and p^1 by the splits (46)-(48) and (43), the effective model parameters can be introduced. Symmetric expressions for the two elasticity tensors are derived using the local problems (49)-(50),

$$\begin{aligned} E_{\alpha\beta\mu\nu}^H &= \oint_{\Xi_S} \mathbb{E} \bar{\nabla}_y^S (\bar{\chi}^{\mu\nu} + \Pi^{\mu\nu}) : \bar{\nabla}_y^S (\bar{\chi}^{\alpha\beta} + \Pi^{\alpha\beta}) , \\ S_{\alpha\beta}^H &= \oint_{\Xi_S} [\mathbf{S} \nabla_y (\chi^\alpha + y_\alpha)] \cdot \nabla_y (\chi^\beta + y_\beta) . \end{aligned} \quad (56)$$

Due to the presence of p^0 in the expression of $\bar{\mathbf{u}}^1$, see (46), a pressure-coupling term appears which involves coefficient \mathbf{H} introduced in (53),

$$\mathrm{i}\omega\rho_0 p^0 \oint_{\Xi_S} (\mathbb{E} \bar{\nabla}_y^S \bar{\chi}^*) : \bar{\nabla}_x^S \bar{\mathbf{v}}^0 = -\mathrm{i}\omega\rho_0 p^0 \mathbf{H} : \bar{\nabla}_x^S \bar{\mathbf{v}}^0 , \quad (57)$$

where the identity follows upon substituting the test functions in (49) and (51) by $\bar{\chi}^*$ and $\bar{\chi}^{\alpha\beta}$, respectively.

In the r.h.s. integrals of (55), the following coefficients $\mathbf{C} = (C_k)$ and $\mathbf{T} = (T_j^k)$ are introduced,

$$\begin{aligned} C_k &= \oint_{I_y^+} \eta^k - \oint_{I_y^-} \eta^k , \\ T_j^k &= - \oint_{\partial S} \eta^k n_j = (\nabla_y \eta^k, \nabla_y \eta^j)_{Y^*} = T_k^j , \quad k, j = 1, 2, 3 , \end{aligned} \quad (58)$$

so that \mathbf{T} is symmetric.

Using the homogenized coefficients, the macroscopic (homogenized) plate equation (55) can be rewritten:

$$\begin{aligned} & -\omega^2 \int_{\Gamma_0} \bar{\rho}_S \left(\mathbf{u}^0 \cdot \mathbf{v} + \frac{h^2}{12} \boldsymbol{\theta}^0 \cdot \boldsymbol{\vartheta} \right) + \int_{\Gamma_0} (\mathbf{S}^H (\bar{\nabla}_x u_3^0 - \boldsymbol{\theta}^0)) \cdot (\bar{\nabla}_x v_3 - \boldsymbol{\vartheta}) \\ & + \frac{h^2}{12} \int_{\Gamma_0} (\mathbb{E}^H \bar{\nabla}_x^S \boldsymbol{\theta}^0) : \bar{\nabla}_x^S \boldsymbol{\vartheta} + \int_{\Gamma_0} (\mathbb{E}^H \bar{\nabla}_x^S \bar{\mathbf{u}}^0) : \bar{\nabla}_x^S \bar{\mathbf{v}} - \mathrm{i}\omega\rho_0 \int_{\Gamma_0} p^0 \mathbf{H} : \bar{\nabla}_x^S \bar{\mathbf{v}} \\ & = \frac{\rho_0}{h} \int_{\Gamma_0} \mathbf{v} \cdot (\mathrm{i}\omega \mathbf{D}^T \bar{\nabla} p^0 - \omega^2 \mathbf{C} g^0 + \omega^2 \mathbf{T} \mathbf{u}^0) , \end{aligned} \quad (59)$$

for all $(\mathbf{v}, \boldsymbol{\vartheta}) \in (H_0^1(\Gamma_0))^5$. Above $\bar{\rho}_S$ is the effective plate density, $\bar{\rho}_S = |\Xi|^{-1} \int_{\Xi_S} \rho$.

4. Global problem with vibroacoustic transmission conditions

We recall the problem decomposition according to (8), (9) and conditions (10). The problem (9) describing the vibro-acoustic response in the layer has been homogenized, yielding equations (70) and (71). Our further effort will focus on the coupling the acoustic field in the layer with the surrounding environment. We consider dilated domains $\hat{\Omega}^\pm$, such that Γ_0 is their common boundary, *i.e.* $\partial\hat{\Omega}^+ \cap \partial\hat{\Omega}^- = \Gamma_0$. By \hat{P} we denote the dilated solutions in domains $\hat{\Omega}^\pm$, the traces of \hat{P} on Γ_0 are denoted by \hat{P}^\pm ; obviously $\hat{P}^+ = \text{trace}_{\Gamma_0}(\hat{P}|_{\hat{\Omega}^+})$ and $\hat{P}^- = \text{trace}_{\Gamma_0}(\hat{P}|_{\hat{\Omega}^-})$.

4.1. Coupling of the layer with external acoustic fields

In this section, we use the convergence result concerning the acoustic potential p^ε , namely (28), and consider coupling of the acoustic fields “inside” the layer with the ones “outside” the layer. In particular, below we introduce a coupling equation (60) which is associated with the limit equations in the homogenized layer and provide the transmission conditions for the global problem.

We recall the condition $P^\delta = \hat{p}^\varepsilon$ on Γ_δ^\pm defined in (8) which is now treated in a weak sense. The jump of the exterior field across the layer with finite $\delta > 0$ is expressed, as follows,

$$\int_{\Gamma_\delta^+} \psi P^\delta - \int_{\Gamma_\delta^-} \psi P^\delta = \int_{\Gamma_0} \psi \int_{-\delta/2}^{\delta/2} \partial_{x_3} \tilde{p}^{\varepsilon\delta} \quad \forall \psi \in L^2(\Gamma_0), \quad (60)$$

where we assume $\psi = \psi(x')$, $x' \in \Gamma_0$, where by $\tilde{\cdot}$ we denote an extension of $p^{\varepsilon\delta}$ to the whole Ω_δ . We may apply the dilation transformation; let $\hat{P}^{\delta+}$ is defined on Γ_0 , such that $\hat{P}^{\delta+}(x', 0) = P^\delta(x', \delta/2)$ and, in analogy, we introduce $\hat{P}^{\delta-}$, consequently (60) can be written,

$$\int_{\Gamma_0} \psi (\hat{P}^{\delta+} - \hat{P}^{\delta-}) = \varepsilon \int_{\Gamma_0} \psi \int_{-\varkappa/2}^{\varkappa/2} \frac{1}{\varepsilon} \partial_z \tilde{p}^\varepsilon \quad \forall \psi \in L^2(\Gamma_0). \quad (61)$$

With reference to Remark 1, we now consider a finite layer thickness $\delta_0 = \varkappa\varepsilon_0 > 0$ in the l.h.s. expression of (61), whereas we pass to the limit on the r.h.s. ; this yields the following approximation

$$\begin{aligned} \frac{1}{\varepsilon_0} \int_{\Gamma_0} \psi (\hat{P}^{\delta+} - \hat{P}^{\delta-}) &\approx \lim_{\varepsilon \rightarrow 0} \int_{\Gamma_0} \psi \int_{-\varkappa/2}^{\varkappa/2} \frac{1}{\varepsilon} \oint_{\Xi} \partial_z \mathcal{T}_\varepsilon(\tilde{p}^\varepsilon) \\ &= \int_{\Gamma_0} \psi \int_{-\varkappa/2}^{\varkappa/2} \oint_{\Xi} \partial_z \tilde{p}^1 = \int_{\Gamma_0} \psi [\![\tilde{p}^1]\!]_{\varkappa}^\pm \\ &= \int_{\Gamma_0} \psi \left(\oint_{I_y^+} p^1 - \oint_{I_y^-} p^1 \right) \quad \forall \psi \in L^2(\Gamma_0). \end{aligned} \quad (62)$$

We substitute the split form of p^1 in (62) which yields new positive coefficient $F > 0$ and two other coefficients \mathbf{B}' , \mathbf{C}' :

$$\begin{aligned} F &= - \oint_{I_y^+} \xi + \oint_{I_y^-} \xi = \oint_{Y^*} \nabla_y \xi \cdot \nabla_y \xi \,, \\ B'_\alpha &= \oint_{I_y^+} \pi^\alpha - \oint_{I_y^-} \pi^\alpha = \oint_{Y^*} \partial_\alpha^y \xi = B_\alpha \,, \quad \alpha = 1, 2 \,, \\ C'_k &= \oint_{I_y^+} \eta^k - \oint_{I_y^-} \eta^k = \oint_{\partial S} n_k \xi = C_k \,, \quad k = 1, 2, 3 \,, \end{aligned} \quad (63)$$

where the equalities $\mathbf{B} = \mathbf{B}'$ and $\mathbf{C} = \mathbf{C}'$ are obtained due to the local microscopic problems (44). Now the limit coupling condition (62) can be written in terms of the homogenized coefficients F , \mathbf{C} and \mathbf{B}

$$\int_{\Gamma_0} \psi (\mathbf{B}' \cdot \overline{\nabla}_x p^0 - i\omega F g^0 + i\omega \mathbf{C}' \cdot \mathbf{u}^0) = \frac{1}{\varepsilon_0} \int_{\Gamma_0} \psi (\hat{P}^{\delta_0+} - \hat{P}^{\delta_0-}) \quad \forall \psi \in L^2(\Gamma_0) \,. \quad (64)$$

Due to the above mentioned symmetry, in (64), coefficients \mathbf{B}' and \mathbf{C}' can be replaced simply by \mathbf{B} and \mathbf{C} , which reveals the symmetry of the system of equations (54), (59) and (64).

A question which arises naturally is how the limit field p^0 defined on Γ_0 is related to traces $\hat{P}^{\delta_0\pm}$ of the global solution in $\Omega_{\delta_0}^\pm$. Recalling again the 2nd condition in (10), we can establish a blending function: $\tilde{P}_\delta(x', z) := (\varkappa/2 + z)\hat{P}_\delta^+ + (z - \varkappa/2)\hat{P}_\delta^-$, where $(x', z) \in \Gamma_0 \times]-\varkappa/2, +\varkappa/2[$ and \hat{P}_δ^\pm has been defined above. Further we consider the following condition (recall that $\hat{\Omega}$ is the dilated layer):

$$\int_{\hat{\Omega}} (\tilde{p}^\varepsilon - \tilde{P}_\delta) \overline{\varphi} = 0 \quad \forall \varphi \in L^2(\Gamma_0), \quad (65)$$

such that $\overline{\varphi}(x', z) = \varphi(x')$ for $x' \in \Gamma_0$. Due to the convergence result (27)₁ and due to the construction of \tilde{P}_δ , in the limit $\varepsilon \rightarrow 0$ we get

$$\int_{\Gamma_0} \left(p^0 - \frac{1}{2} [\hat{P}^+ + \hat{P}^-] \right) \varphi = 0 \quad \forall \varphi \in L^2(\Gamma_0) \,. \quad (66)$$

Recalling the finite thickness δ_0 , this equation can be interpreted for $\hat{P}^\pm \approx \hat{P}_{\delta_0}^\pm$, as in the case of the coupling condition (62). By virtue of the r.h.s. integral in (64), for a later use we introduce ΔP , so that due to (66) p^0 is expressed, as follows,

$$\begin{aligned} \Delta P &= \frac{1}{\varepsilon_0} (\hat{P}^+ - \hat{P}^-) \,, \\ p^0 &= \frac{1}{2} (\hat{P}^+ + \hat{P}^-) \,. \end{aligned} \quad (67)$$

4.2. Vibro-acoustic problem in the homogenized layer

We shall summarize the limit equations of the homogenized transmission layer problem arising from the problem constituted by equations (20)-(21) and with the imposed acoustic momentum fluxes $\hat{g}^{\varepsilon\pm}$ given in the form (22).

As announced in the introduction, the homogenized Reissner-Mindlin plate model is valid for “*simple*” perforations generated by cylindrical holes $\partial_o\Sigma$ defined according to (3), being generated by surface $\partial_o S$, see (7). This leads to various simplifications which have already been respected when deriving the homogenized model. Moreover, from the microscopic problems (44), due to Remark 2, the following cancellations can be deduced due to the special geometry, in particular

$$\begin{aligned} C_1 = C_2 = 0, \quad C_3 &= \oint_{\partial S} n_3 \xi, \\ D_3^\alpha &= 0, \quad D_k^\alpha = \oint_{\partial S} n_k \pi^\alpha, \quad k = 1, 2, \alpha = 1, 2, \\ B_\alpha &= 0, \quad \alpha = 1, 2, \end{aligned} \tag{68}$$

where the last identity has already been observed in [14], dealing with rigid plates.

Remark 3. For rigid plates, the plate deflections and rotations disappear. Thus, equation (59) is irrelevant and, hence, coefficients \mathbf{P} and \mathbf{C} and \mathbf{H} are not involved in (64) and (54). However, quite general types of perforations can be considered for which coefficients B_α do not vanish.

△

To rewrite the resulting equations in a more convenient form, we introduce the inner product notation:

$$\langle \phi, \psi \rangle_{\Gamma_0} = \int_{\Gamma_0} \phi \psi.$$

By virtue of the r.h.s. integral in (54), we shall use

$$\Delta G^1(x') := \frac{1}{|\Xi|} \oint_{\Xi} \Delta g^1(x', y') dy', \quad x' \in \Gamma_0, \tag{69}$$

where $\Delta g^1 = g^{1+} - g^{1-}$ has been introduced above.

Assume for a while that ΔP and ΔG^1 are given on Γ_0 . Then, since $B_\alpha = 0$, the model constituted by (54), (59) and (64) would yield two separate problems which are described in the next two sections. Also we recall the relationship between the plate thickness h and the perforation size ε_0 , $h = \varepsilon_0 \bar{h}$, whereby $\delta_0 = \varepsilon_0 \varkappa$ determines the actual transmission layer thickness.

4.2.1. Tangential acoustic wave coupled with in-plane plate vibration

The first subproblem arising from (59) and (54) is independent of the jump ΔP . As explained below, it couples in-plane plate vibrations described by $\bar{\mathbf{u}}^0$ with surface acoustic waves propagating in the fluid in the tangential direction w.r.t. the plate, thus, being described by the acoustic potential p^0 .

To obtain a symmetric system, we multiply (59) by factor \bar{h}/ρ_0 and consider $v_3 = 0$ and $\vartheta_\alpha = 0$. The fluid equation (54) is multiplied by $1/c^2$. The following separate problem can be distinguished: For a given $\Delta G^1 \in L^2(\Gamma_0)$, find $(p^0, \bar{\mathbf{u}}^0) \in H^1(\Gamma_0) \times (H_0^1(\Gamma_0))^2$ such that (by $\bar{\mathbf{I}} = (\delta_{ij})$ we denote the 2D identity)

$$\begin{aligned} & \langle \mathbf{A} \bar{\nabla} p^0, \bar{\nabla} q \rangle_{\Gamma_0} - \omega^2 \left\langle \left(\frac{\zeta^*}{c^2} + \rho_0 K \right) p^0, q \right\rangle_{\Gamma_0} \\ & + i\omega \left(\langle \mathbf{D} \bar{\mathbf{u}}^0, \bar{\nabla} q \rangle_{\Gamma_0} + \bar{h} \left\langle \mathbf{H} : \bar{\nabla}^S \bar{\mathbf{u}}^0, q \right\rangle_{\Gamma_0} \right) = -i\omega \langle \Delta G^1, q \rangle_{\Gamma_0} , \\ & -i\omega \left(\langle \bar{\nabla} p^0, \mathbf{D} \bar{\mathbf{v}} \rangle_{\Gamma_0} + \bar{h} \left\langle p^0, \mathbf{H} : \bar{\nabla}^S \bar{\mathbf{v}} \right\rangle_{\Gamma_0} \right) \\ & + \frac{\bar{h}}{\rho_0} \left\langle \mathbb{E}^H \bar{\nabla}^S \bar{\mathbf{u}}^0, \bar{\nabla}^S \bar{\mathbf{v}} \right\rangle_{\Gamma_0} - \omega^2 \left\langle \left(\frac{\bar{h} \bar{\rho}_S}{\rho_0} \bar{\mathbf{I}} + \bar{\mathbf{T}} \right) \bar{\mathbf{u}}^0, \bar{\mathbf{v}} \right\rangle_{\Gamma_0} = 0 , \end{aligned} \tag{70}$$

for all $(q, \bar{\mathbf{v}}) \in H^1(\Gamma_0) \times (H_0^1(\Gamma_0))^2$.

4.2.2. Plate deflection coupled with transversal acoustic momentum

The second subproblem governs the transversal plate vibrations described by the couple $(u_3^0, \boldsymbol{\theta}^0)$ with the transversal acoustic momentum g^0 of the fluid in response to a given jump ΔP , whereas ΔG^1 is not involved. We consider $v_\alpha = 0$ and $\alpha = 1, 2$ in (59) which again is multiplied by factor \bar{h}/ρ_0 . The resulting equation is coupled with (64) multiplied by $i\omega$, so that the following separate problem can be distinguished: For a given $\Delta P \in L^2(\Gamma_0)$ find $(g^0, u_3^0, \boldsymbol{\theta}^0) \in L^2(\Gamma_0) \times (H_0^1(\Gamma_0))^3$ such that

$$\begin{aligned} & -\omega^2 \langle F g^0, \psi \rangle_{\Gamma_0} + \omega^2 \langle C_3 u_3^0, \psi \rangle_{\Gamma_0} = i\omega \langle \Delta P, \psi \rangle_{\Gamma_0} , \\ & \omega^2 \langle g^0, C_3 v_3 \rangle_{\Gamma_0} - \omega^2 \left\langle \left(\frac{\bar{h} \bar{\rho}_S}{\rho_0} + T_{33} \right) u_3^0, v_3 \right\rangle_{\Gamma_0} - \omega^2 \frac{\bar{h} h^2}{12 \rho_0} \left\langle \frac{\bar{\rho}_S}{\rho_0} \boldsymbol{\theta}^0, \boldsymbol{\vartheta} \right\rangle_{\Gamma_0} \\ & + \frac{\bar{h}}{\rho_0} \left\langle \mathbf{S}^H (\bar{\nabla} u_3^0 - \boldsymbol{\theta}^0), \bar{\nabla} v_3 - \boldsymbol{\vartheta} \right\rangle_{\Gamma_0} + \frac{\bar{h} h^2}{12 \rho_0} \left\langle \mathbb{E}^H \bar{\nabla}^S \boldsymbol{\theta}^0, \bar{\nabla}^S \boldsymbol{\vartheta} \right\rangle_{\Gamma_0} = 0 , \end{aligned} \tag{71}$$

for all $(\psi, v_3, \boldsymbol{\vartheta}) \in L^2(\Gamma_0) \times (H_0^1(\Gamma_0))^3$.

4.2.3. Rigid plate with general shape of perforations

Assuming arbitrary shaped pores perforating the plate allowing for a more general geometry of the fluid cell Y^* and leading to a nonsymmetry of the response ξ , see [14], (54) is coupled with (64). For a given $\Delta P \in L^2(\Gamma_0)$ and $\Delta G^1 \in L^2(\Gamma_0)$, find a couple $(p^0, g^0) \in H^1(\Gamma_0) \times L^2(\Gamma_0)$, such that

$$\begin{aligned} \int_{\Gamma_0} (\mathbf{A} \bar{\nabla}_x p^0) \cdot \bar{\nabla}_x q - \zeta^* \frac{\omega^2}{c^2} \int_{\Gamma_0} p^0 q + i\omega \int_{\Gamma_0} g^0 \mathbf{B} \cdot \bar{\nabla}_x q &= -i\omega \int_{\Gamma_0} q \Delta G^1, \\ \int_{\Gamma_0} \psi (\mathbf{B} \cdot \bar{\nabla}_x p^0 - i\omega F g^0) &= \int_{\Gamma_0} \psi \Delta P, \end{aligned} \quad (72)$$

for all $(q, \psi) \in H^1(\Gamma_0) \times L^2(\Gamma_0)$. Thus, both ΔP and ΔG^1 are involved.

4.3. Dirichlet-to-Neumann (DtN) operator and the transmission conditions

For a given $\varepsilon_0 > 0$, by virtue of the approximation introduced above, let us consider a problem arising from (8) for $\delta \rightarrow 0$. The interface condition is now replaced by

$$\frac{\partial \hat{P}|_{\hat{\Omega}^\pm}}{\partial n^\pm} \approx \frac{\partial \hat{P}^{\delta_0 \pm}}{\partial n^\pm} = i\omega \int_{\Xi} \mathcal{T}_{\varepsilon_0}(\hat{g}^{\varepsilon_0, \pm}) \quad \text{on } \Gamma_0, \quad (73)$$

where $\frac{\partial p}{\partial n} = \mathbf{n} \cdot \nabla p$ denotes the normal derivative of p on Γ_0 ; note that $\mathbf{n}^+ = -\mathbf{n}^-$ is outward to $\hat{\Omega}^+$. Therefore, we introduce the averaged momentum fluxes \hat{G}_0^\pm defined by averaging the unfolded expressions (22) over the period Ξ , so that

$$\begin{aligned} \hat{G}_0^\pm(x') &= \pm \frac{1}{|\Xi|} \int_{\Xi} \mathcal{T}_{\varepsilon_0}(\hat{g}^{\varepsilon_0, \pm}) = \frac{1}{|\Xi|} \int_{\Xi} (g^0(x') + \varepsilon_0 g^{1, \pm}(x', y')) dy' \\ &= g^0(x') + \varepsilon_0 G^{1\pm}(x'), \quad \text{where } G^{1\pm} = \frac{1}{|\Xi|} \int_{\Xi} g^{1\pm}(x', y') dy'. \end{aligned} \quad (74)$$

Hence

$$\begin{aligned} g^0 &\approx \frac{1}{2} (\hat{G}_0^+ + \hat{G}_0^-) = g^0 + \frac{\varepsilon_0}{2} (G^{1+} + G^{1-}), \\ \Delta G^1 &= G^{1+} - G^{1-} = \frac{1}{\varepsilon_0} (\hat{G}_0^+ - \hat{G}_0^-), \end{aligned} \quad (75)$$

where ΔG^1 was defined in (69) with $\Delta g^1 = g^{1,+} - g^{1,-}$. Moreover, if we assume that $G^{1+} = -G^{1-}$, then equality holds in (75)₁ for any ε_0

Now for a while, we may consider the following problem: For given \bar{p} , \hat{G}_0^+ and \hat{G}_0^- , find \hat{P} in Ω^G satisfying

$$\begin{aligned}
& c^2 \nabla^2 \hat{P} + \omega^2 \hat{P} = 0 \quad \text{in } \hat{\Omega}^+ \cup \hat{\Omega}^- , \\
& \textbf{interface condition:} \\
& \frac{\partial \hat{P}|_{\hat{\Omega}^+}}{\partial n^+} = i\omega \hat{G}_0^+ \quad \text{on } \Gamma_0 , \\
& \frac{\partial \hat{P}|_{\hat{\Omega}^-}}{\partial n^-} = -i\omega \hat{G}_0^- \quad \text{on } \Gamma_0 , \\
& \text{outer boundary conditions}
\end{aligned} \tag{76}$$

$$ri\omega c \hat{P} + c^2 \frac{\partial \hat{P}}{\partial n} = s2i\omega c \bar{p} \quad \text{on } \partial_{\text{ext}} \Omega^G .$$

see problem (8) concerning constants r and s involved in the boundary conditions on $\partial_{\text{ext}} \Omega^G$.

Problem (76) arises from (8) for $\delta \rightarrow 0$, however, the Dirichlet type interface conditions are now replaced by the Neumann ones represented by (73) with (74).

Problem (76), as well as problems (70) and (71) are artificial; in fact, neither \hat{G}_0^\pm , nor ΔP or ΔG^1 are known a priori; they all are coupled to the solution \hat{P} due to the interface vibroacoustic interaction conditions (70) and (71) which involve ΔP , g^0 and ΔG^1 . While g^0 and ΔG^1 are related to \hat{G}_0^\pm directly by (75), ΔP and p^0 are related to traces \hat{P}^\pm by (67).

The problems (70) and (71), and the conditions (67) and (75) present an implicit form of the *Dirichlet-to-Neumann operator* (DtN) associated with the “outer” acoustic problem defined for \hat{P} in $\hat{\Omega}^\pm$.

4.4. Global acoustic problem with homogenized perforated plate

In order to write the weak formulation of problem (76) with the DtN mapping introduced above, we shall employ the following bilinear forms involving

the homogenized coefficients introduced in the preceding sections,

$$\begin{aligned}
\mathcal{A}(p, q) &= \langle \mathbf{A} \bar{\nabla} p, \bar{\nabla} q \rangle_{\Gamma_0} , \\
\mathcal{S}((w, \boldsymbol{\theta}), (v, \boldsymbol{\vartheta})) &= \frac{\bar{h}}{\rho_0} \langle \mathbf{S}^H (\bar{\nabla} w - \boldsymbol{\theta}), \bar{\nabla} v - \boldsymbol{\vartheta} \rangle_{\Gamma_0} , \\
\mathcal{E}(\boldsymbol{\theta}, \boldsymbol{\vartheta}) &= \frac{\bar{h}}{\rho_0} \langle \mathbb{E}^H \bar{\nabla}^S \boldsymbol{\theta}, \bar{\nabla}^S \boldsymbol{\vartheta} \rangle_{\Gamma_0} , \\
\mathcal{F}(g, \psi) &= \langle Fg, \psi \rangle_{\Gamma_0} , \\
\mathcal{H}(\bar{\mathbf{v}}, p) &= \bar{h} \langle \mathbf{H} : \bar{\nabla}^S \bar{\mathbf{v}}, p \rangle_{\Gamma_0} , \\
\mathcal{C}(u, \psi) &= \langle C_3 u, \psi \rangle_{\Gamma_0} , \\
\mathcal{K}(p, q) &= \left\langle \left(\frac{\zeta^*}{c^2} + \rho_0 K \right) p, q \right\rangle_{\Gamma_0} , \\
\mathcal{L}(\boldsymbol{\theta}, \boldsymbol{\vartheta}) &= \frac{\bar{h}}{\rho_0} \left\langle \frac{\bar{\rho}_S}{\rho_0} \boldsymbol{\theta}, \boldsymbol{\vartheta} \right\rangle_{\Gamma_0} , \\
\mathcal{M}(\bar{\mathbf{u}}, \bar{\mathbf{v}}) &= \left\langle \left(\frac{\bar{h} \bar{\rho}_S}{\rho_0} \bar{\mathbf{I}} + \bar{\mathbf{T}} \right) \bar{\mathbf{u}}, \bar{\mathbf{v}} \right\rangle_{\Gamma_0} , \\
\mathcal{N}(u, z) &= \left\langle \left(\bar{h} \frac{\bar{\rho}_S}{\rho_0} + T_{33} \right) u, z \right\rangle_{\Gamma_0} , \\
\mathcal{D}(\bar{\mathbf{v}}, p) &= \langle \mathbf{D} \bar{\mathbf{v}}, \bar{\nabla} p \rangle_{\Gamma_0} , \\
\mathcal{B}(p, \psi) &= \langle \mathbf{B} \cdot \bar{\nabla} p, \psi \rangle_{\Gamma_0} .
\end{aligned} \tag{77}$$

Above the bilinear forms $\mathcal{F}, \mathcal{C}, \mathcal{N}$ and \mathcal{M} are related to the inertia and fluid-structure interaction effects, while \mathcal{S} and \mathcal{E} are related to the plate stiffness.

The global acoustic field $\hat{P} \in H^1(\hat{\Omega}^+ \cup \hat{\Omega}^-)$ satisfies

$$\begin{aligned}
&c^2 \int_{\hat{\Omega}^+ \cup \hat{\Omega}^-} \nabla \hat{P} \cdot \nabla Q - \omega^2 \int_{\hat{\Omega}^+ \cup \hat{\Omega}^-} \hat{P} Q + \int_{\partial_{\text{ext}} \Omega^G} r i \omega c \hat{P} Q \\
&- i \omega c^2 \left(\left\langle \hat{G}_0^+, Q^+ \right\rangle_{\Gamma_0} - \left\langle \hat{G}_0^-, Q^- \right\rangle_{\Gamma_0} \right) = \int_{\partial_{\text{ext}} \Omega^G} s i \omega c \bar{p} Q
\end{aligned} \tag{78}$$

for all $Q \in H^1(\hat{\Omega}^+ \cup \hat{\Omega}^-)$, whereby Q^\pm denotes the trace of Q on $\partial \hat{\Omega}^\pm$.

The DtN operator involving functions $(\hat{P}^\pm, p^0, \bar{\mathbf{u}}) \in [L^2(\Gamma_0)]^2 \times H^1(\Gamma_0) \times [H_0^1(\Gamma_0)]^2$ and $(\hat{G}_0^\pm, u_3, \boldsymbol{\theta}) \in [L^2(\Gamma_0)]^2 \times H_0^1(\Gamma_0) \times [H_0^1(\Gamma_0)]^2$ is represented by the following equalities arising from (70) and (71) where we employ (67) and

(75), so that we have

$$\begin{aligned} \mathcal{A}(p^0, q) - \omega^2 \mathcal{K}(p^0, q) + i\omega (\mathcal{D}(\bar{\mathbf{u}}, q) + \mathcal{H}(\bar{\mathbf{u}}, q)) + \frac{i\omega}{\varepsilon_0} \left\langle [\hat{G}_0^+ - \hat{G}_0^-], q \right\rangle_{\Gamma_0} &= 0, \\ -i\omega (\mathcal{D}(\bar{\mathbf{v}}, p^0) + \mathcal{H}(\bar{\mathbf{v}}, p^0)) + \mathcal{E}(\bar{\mathbf{u}}, \bar{\mathbf{v}}) - \omega^2 \mathcal{M}(\bar{\mathbf{u}}, \bar{\mathbf{v}}) &= 0, \end{aligned} \quad (79)$$

for all $(q, \bar{\mathbf{v}}) \in H^1(\Gamma_0) \times [H_0^1(\Gamma_0)]^2$, and

$$\begin{aligned} \frac{\omega^2}{2} \mathcal{F}([\hat{G}_0^+ + \hat{G}_0^-], \psi) - \omega^2 \mathcal{C}(u_3, \psi) + \frac{i\omega}{\varepsilon_0} \left\langle [\hat{P}^+ - \hat{P}^-], \psi \right\rangle_{\Gamma_0} &= 0, \\ \frac{\omega^2}{2} \mathcal{C}([\hat{G}_0^+ + \hat{G}_0^-], v_3) - \omega^2 \left(\mathcal{N}(u_3, v_3) + \frac{h^2}{12} \mathcal{L}(\boldsymbol{\theta}, \boldsymbol{\vartheta}) \right) & \\ + \mathcal{S}((u_3, \boldsymbol{\theta}), (v_3, \boldsymbol{\vartheta})) + \frac{h^2}{12} \mathcal{E}(\boldsymbol{\theta}, \boldsymbol{\vartheta}) &= 0, \end{aligned} \quad (80)$$

for all $(\psi, v, \boldsymbol{\vartheta}) \in L^2(\Gamma_0) \times H_0^1(\Gamma_0) \times [H_0^1(\Gamma_0)]^2$. There is the coupling equation:

$$\left\langle 2p^0 - [\hat{P}^+ + \hat{P}^-], q \right\rangle_{\Gamma_0} = 0 \quad \forall q \in L^2(\Gamma_0). \quad (81)$$

Now we can state the main result of the paper.

Global acoustic problem with the homogenized perforated plate. Given the incident acoustic wave represented by \bar{p} on Γ_{in} , find the acoustic potential \hat{P} defined in $\hat{\Omega}^G = \hat{\Omega}^+ \cup \hat{\Omega}^-$ and other functions $(p^0, \hat{G}_0^\pm, \mathbf{u}, \boldsymbol{\theta})$ defined on Γ_0 such that the variational equalities (78)-(81) hold.

Remark 4. It is left as an easy excersie for raders that, if a rigid plate is considered, the model reduces. From (72), insetad of (79) and (80), the DtN operator is established in terms of \hat{P}^\pm and (p^0, \hat{G}_0^\pm) which satisfy the following variational equalities,

$$\begin{aligned} \mathcal{A}(p^0, q) - \omega^2 \mathcal{K}_R(p^0, q) + \frac{i\omega}{2} \mathcal{B}(q, [\hat{G}_0^+ + \hat{G}_0^-]) + \frac{i\omega}{\varepsilon_0} \left\langle [\hat{G}_0^+ - \hat{G}_0^-], q \right\rangle_{\Gamma_0} &= 0, \\ \frac{\omega^2}{2} \mathcal{F}([\hat{G}_0^+ + \hat{G}_0^-], \psi) + i\omega \mathcal{B}(p^0, \psi) - \frac{i\omega}{\varepsilon_0} \left\langle [\hat{P}^+ - \hat{P}^-], \psi \right\rangle_{\Gamma_0} &= 0, \end{aligned} \quad (82)$$

for all $(q, \psi) \in H^1(\Gamma_0) \times L^2(\Gamma_0)$, whereby (67) holds. Note that \mathcal{K}_R is defined according to (77), but with $K = 0$, whereby \mathcal{B} vanishes for simple perforations.

△

5. Validation of the homogenized model

The homogenized model derived in this paper provides an approximation of the vibroacoustic interaction in a vicinity of the perforated plate. This approximation is introduced as the limit behaviour of the wave propagation in the heterogeneous structure when the transmission layer thickness and the characteristic size of the perforations diminish with $\varepsilon \rightarrow 0$. However, by virtue of coupling the limit layer model (54) and (59) with the “outer” acoustic problem, the Global problem described in Section 4 is featured by the specific scale parameter ε_0 associated with a given plate thickness and the perforation size. In this section, we examine how numerical responses of the proposed homogenized vibroacoustic model corresponds with solutions of the “original” problem (1) associated with the 3D heterogeneous solid structure representing the plate.

To this aim, the reference model is established as the finite element (FE) approximation of problem introduced in Section 2. For this model, the heterogeneous structure of the transmission layer is built up as the periodic lattice by copies of the reference periodic cell according to (3)-(4). The geometries associated with the homogenized and the reference models are illustrated in Fig. 5, where the unit cell Y^* represents the fluid domain. By virtue of the asymptotic homogenization, the layer presenting a “fictitious” interface, highlighted by red and blue colors in Fig 5(left), is replaced by homogenized transmission conditions imposed on the interface Γ_0 in the multiscale simulation, see Fig 5(right).

The validation of the homogenized model (78)-(81) is performed in two steps. First, we compare the acoustic fields computed by the reference and the homogenized models, whereby the perforated plate is assumed to be rigid, see Remark 4. Secondly we compare the responses of the homogenized vibrating plate with the deflections obtained by direct numerical simulations (DNS) of the heterogeneous 3D elastic structure. In this case, the plate surface is loaded by a given acoustic pressure distribution, thus, the vibroacoustic problem is decoupled. The reason for such a simplification arises as the consequence of the FE mesh complexity increasing with the number of the perforating holes, thus, inducing a discretized problem with large number of the degrees of freedom (DOFs).

For the purpose of this validation test, we consider the waveguide Ω represented by the “S”-shaped slice of thickness $\varepsilon_0 m$, as measured in the x_2 -axis direction, see Fig. 4, where the slice dimensions are indicated. The waveguide is symmetric w.r.t. the center of the perforated plate structure which splits the acoustic domain into two mutually symmetric parts. The thickness of the perforated plate is $0.12\varepsilon_0 m$, where $\varepsilon_0 = 0.3/N$ varies with N ,

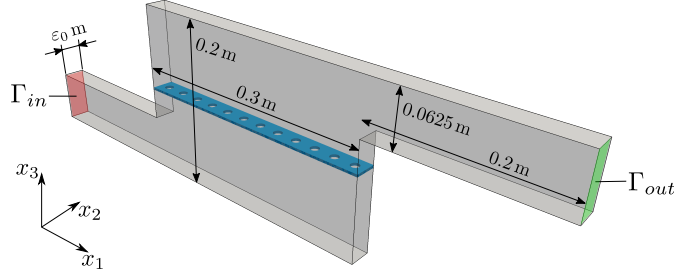


Figure 4: The acoustic domain with the embedded perforated plate.

the number of the perforation periods (holes) drawn in the x_1 -axis direction.

The homogenized models and the reference model presented in this paper have been implemented in *SfePy* – Simple Finite Elements in Python [2], a software developed for an efficient solving of multiscale problems by means of the finite element method. In the validation tests and the coupled problem simulation, by the “multiscale simulations” we mean solutions of the homogenized (macroscopic) problem supplemented by the reconstruction procedure which allows us to respect the local fluctuations superimposed to the solutions of the macroscopic problem when the scale parameter ε_0 is given.

5.1. Validation test – acoustic field in fluid

In this test, the perforated plate is rigid, so that the distribution of the reference acoustic pressure field is governed by equations (1) modified for the rigid plate, i.e. $\mathbf{u} = 0$ in Σ . Accordingly, the homogenized layer presents the coupling conditions (82) for the acoustic field in the wave guide which is governed by (78). Recall that the homogenized coefficients \mathbf{A} , \mathbf{B} , F are given by expressions (53), (63) involving solutions of the local problems (44) defined in Y^* .

For both the homogenized and the reference models an incident wave with amplitude $\bar{p} = 300$ Pa is imposed on Γ_{in} , whereby the anechoic condition on Γ_{out} is considered. The periodic conditions are prescribed on the two faces orthogonal to the x_2 -axis direction (front and back faces of the waveguide) for the geometry depicted in Fig. 4.

Responses of the reference and the homogenized models are compared using the global acoustic properties expressed by the transmission loss (TL), and by the local distributions of the acoustic pressure. These responses were computed for the fluid characterized by the acoustic speed $c = 343$ m/s, the density $\rho_0 = 1.2$ kg m³.

The TL curves obtained for both the models are compared in Fig. 6. Perforations with cylindrical holes were examined for two radii r . Results

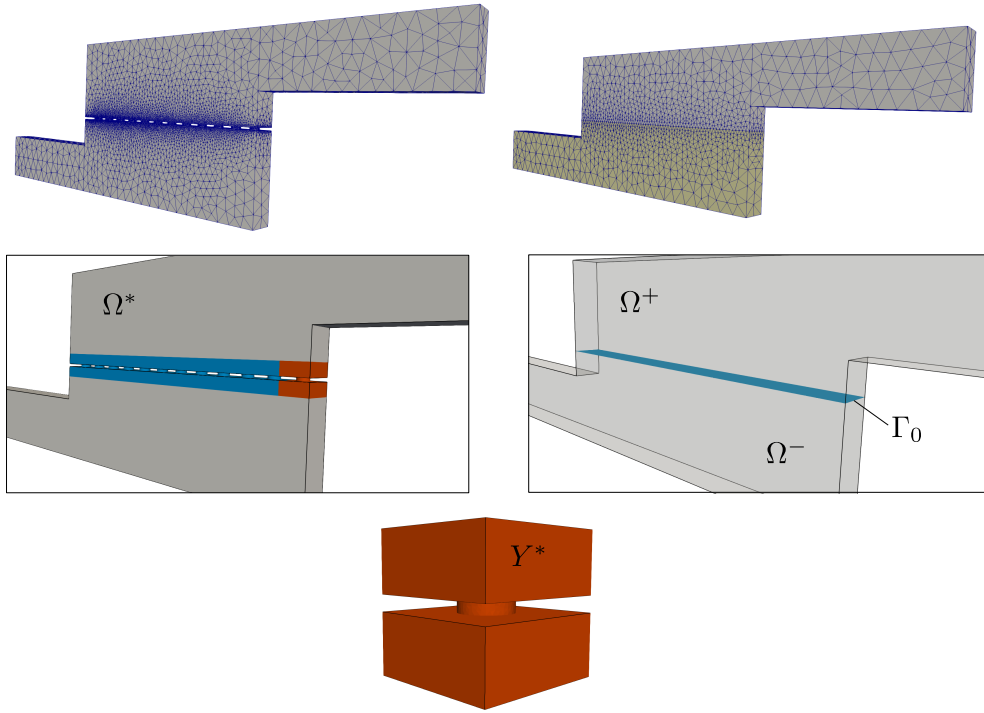


Figure 5: Geometries and FE meshes of the fluid domains related to the reference (left) and homogenized (right) models. Geometry of the periodic cell (bottom) employed in the multiscale simulation and in construction of the reference geometry.

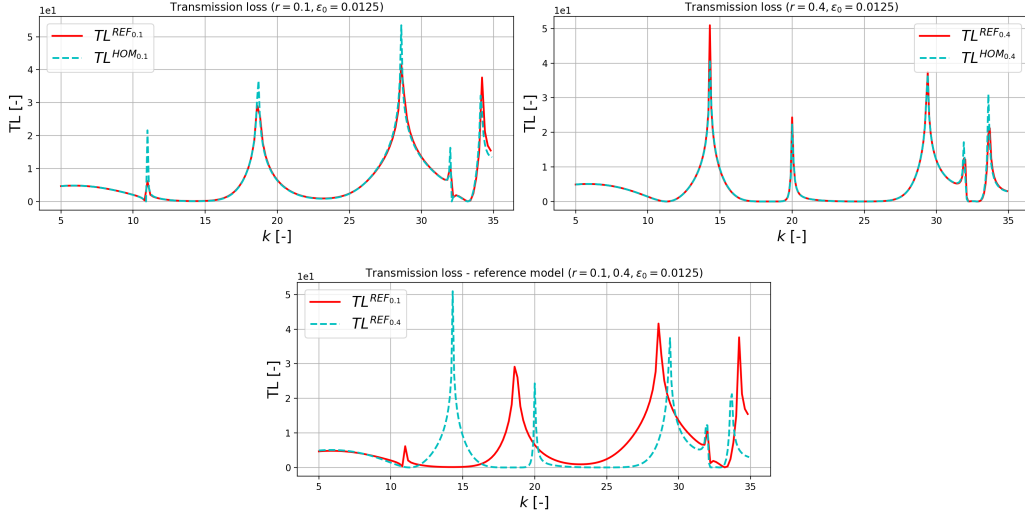


Figure 6: Transmission loss curves for the perforations with the hole radius of $r = 0.1\varepsilon_0$ m and $r = 0.4\varepsilon_0$ m obtained by the reference (*REF*) and homogenized (*HOM*) models, $N = 24$.

for $r = 0.1\varepsilon_0$ m are depicted in Fig. 6(a) and for $r = 0.4\varepsilon_0$ m in Fig. 6(b). From these graphs it is apparent that the results differ only in the vicinity of wave numbers yielding the *TL* peaks; in those regions associated with higher wave numbers also the shift of the peak positions can be observed. However, this effect can be caused by different FE discretizations of both the models. The difference of the two *TL* curves is displayed in Fig. 6(c) for the two dimensions of the holes. The calculations are performed for an interval of the wave number $k \in [5, 35]$ and for $\varepsilon_0 = 0.0125$ which corresponds to $N = 24$.

We also examined responses of the two models in terms of the acoustic fields fluctuations in the wave guide near to and far from the perforated plate. For this, the acoustic pressure distributions were traced along lines l_1 and l_2 , see Fig. 7(top). Line l_2 has a fixed place outside the fictitious layer while l_1 lies in the layer, so that its position depends on ε_0 . We perform a series of calculations for perforations with holes of radii $r = 0.1\varepsilon_0$ and wave number $k = 28$, whereby $\varepsilon_0 = 0.3/N$ varies for $N = 12, 24, 48, 72, 96$. The real parts of the acoustic pressure fields are compared in Fig. 7, distributions of the imaginary parts are similar as the real parts. The pressure field p^{HOM} is reconstructed using the results of the multiscale simulation and the expressions introduced in Appendix A.2. We define the relative pressure error associated with a given line l as $p_{err} := \left| \|p^{REF}\|_l - \|p^{HOM}\|_l \right| / \|p^{REF}\|_l$, where $\|\cdot\|_l$ is the $L^2(l)$ -norm which is well defined due to the conforming

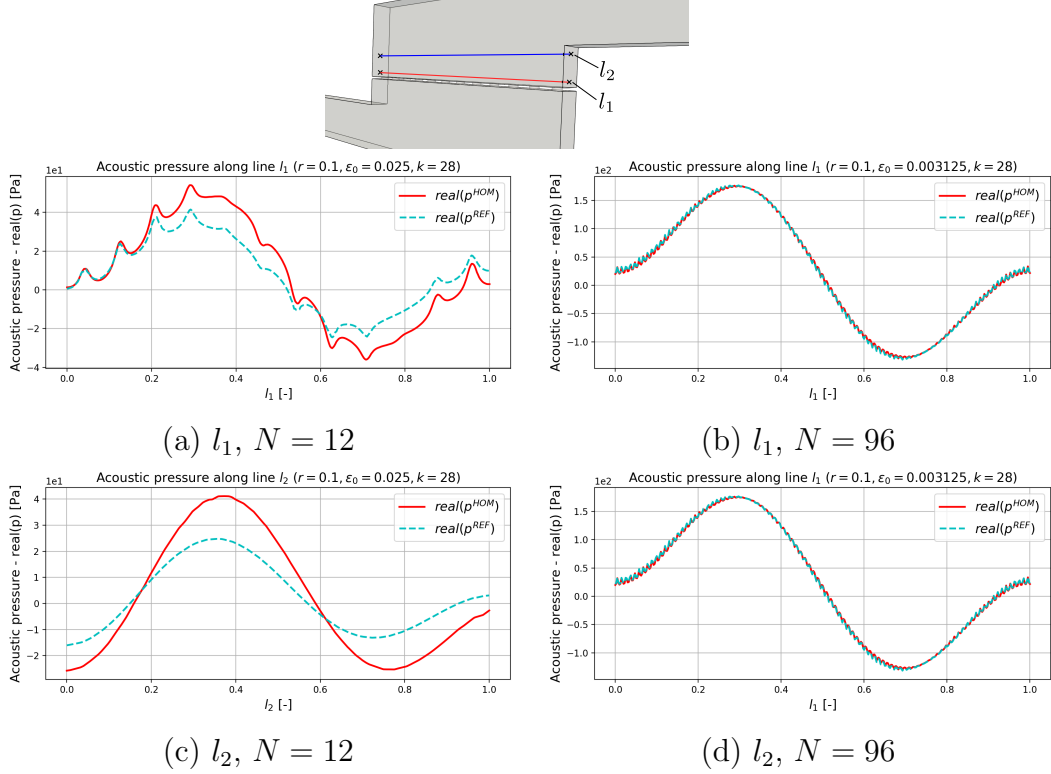


Figure 7: The real parts of the acoustic pressure along lines l_1 (a,b), l_2 (c,d) obtained by the reference (p^{REF}) and homogenized (p^{HOM}) models for $N = 12$ (a,c) and $N = 96$ (b,d), holes with radius $r = 0.1\epsilon_0$ m.

FE approximation of p . This error is illustrated in Fig. 8 for the increasing number of perforations N . It can be seen that p_{err} on both lines l_1 and l_2 is quite high, above 16%, for $N = 12$, however, with growing N the error decreases down to $\approx 1\%$ for $N = 96$. The relative pressure error distribution in the whole domain Ω is shown for $N = 24$ in Fig. 9 (right), the left figure shows the distribution of the pressure p^{REF} .

5.2. Validation test – compliant perforated plate

The second part of the validation test concerns the homogenized model of a perforated plate of the Reissner-Mindlin type. The aim is to compare responses of the homogenized plate model with the ones of the associated 3D elastic structure with the geometry depicted in Fig. 10. This structure representing the plate is loaded on its top surface Γ_{top} by a prescribed complex loading traction stress, see Fig. 11, which mimics the action of the acoustic pressure, so that the loading traction is applied in the out-of-plane direction, axis x_3 . The perforated plate is fixed at its both ends: $\mathbf{u} = \mathbf{0}$ on Γ_{left}

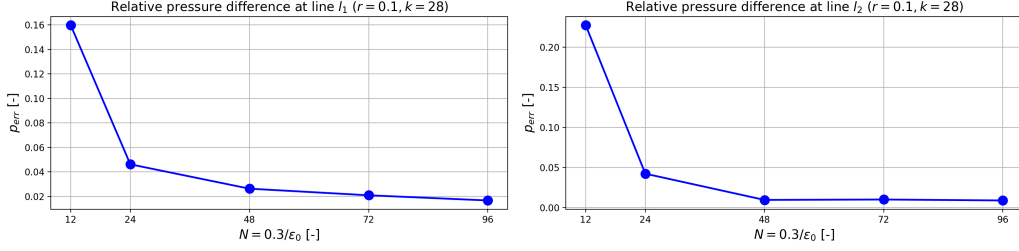


Figure 8: Change of the relative pressure error p_{err} at lines l_1 (left) and l_2 (right) with the increasing number of perforations.

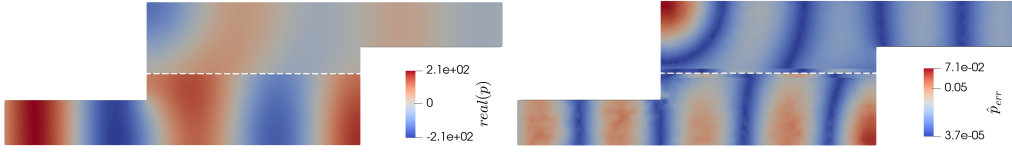


Figure 9: Distribution of the acoustic pressure (left) and the relative pressure error \hat{p}_{err} (right).

and Γ_{right} , and the periodic boundary conditions are applied in the x_2 -axis direction, as it is considered in the acoustic problem above. The equivalent boundary conditions and loading function are used in the homogenized model, where the 3D structure is represented by the plate model described as a 2D structure, see Fig. 10. The material properties of the plate are given by the Young modulus $E = 70 \text{ GPa}$, the Poisson ration $\nu = 0.35$, and by the density $\rho = 2700 \text{ kg m}^3$.

The plate deflections are computed for the two models, *i.e.* using the DNS of the 3D structure and using the multiscale simulations of the plate. The responses are compared for a fixed wave number $k = 28$, where $\varepsilon_0 = 0.3/24$, and for $r = 0.1\varepsilon_0 \text{ m}$ and $r = 0.4\varepsilon_0 \text{ m}$. As seen in Fig. 12, the difference of the

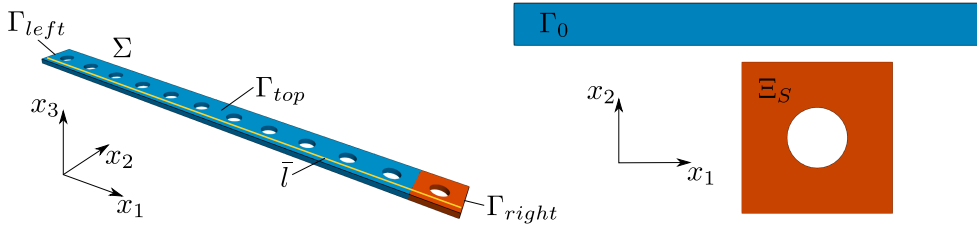


Figure 10: Left: The 3D elastic structure Σ is used in the direct numerical simulation (DNS) as the plate representation; responses depicted in Fig. 12 are compared using traces of solutions on the line $\bar{l} \in \Gamma_{top}$. Right: Geometric 2D representation of the Reissner-Mindlin perforated plate.

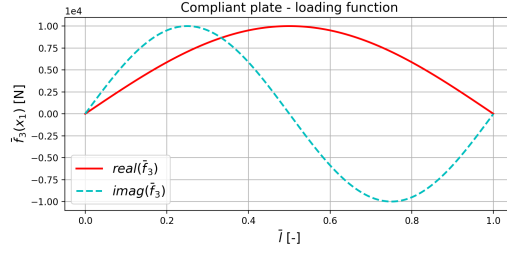


Figure 11: Loading function \bar{f}_3 applied to the compliant plate in the x_3 -axis direction.

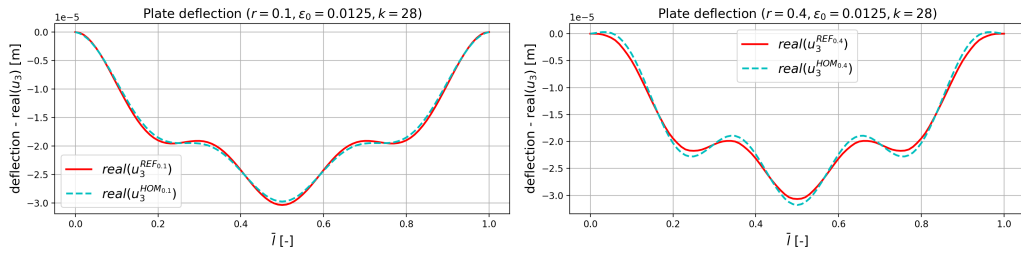


Figure 12: The real parts of the plate deflection along the central line \bar{l} of domains Σ (u_z^{REF}) and Γ_0 (u_z^{HOM}) for $r = 0.1\epsilon_0$ m (left) and $r = 0.4\epsilon_0$ m (right), $N = 24$.

results is less than 5%, even for the relatively small number of perforations $N = 24$. The values are plotted along line \bar{l} which is parallel to axis x_1 , as shown in Fig. 10 left.

The effect of the plate compliance is illustrated in Fig. 13, where we compare the values computed for the rigid and compliant perforated interfaces. The relative difference of the values is defined as $TL_{diff} = |TL^{rigid} - TL^{compl}| / TL^{rigid}$. The influence of the plate compliance on the transmission loss in the waveguide is sensitive on frequency intervals, nevertheless this phenomenon will deserve a further study.

6. Coupled numerical simulation

The purpose of this part is to illustrate, how the homogenized vibroacoustic transmission model derived in this paper can be used for numerical simulations. acoustic waves using the two-scale in this paper. To this aim we consider an analogous problem as the one specified in Section 5.1, whereby the mathematical model given by the coupled equations (78)-(81). The geometry of the waveguide Ω^G is depicted in Fig. 14(top). The boundary conditions at the inlet and outlet parts of the domain boundary, Γ_{in} and Γ_{out} , are defined as in the validation test reported in Section 5.1. On the rest of the boundary $\partial(\hat{\Omega}^+ \cup \hat{\Omega}^-)$ represents the rigid wall, thus, for the acoustic pressure field the

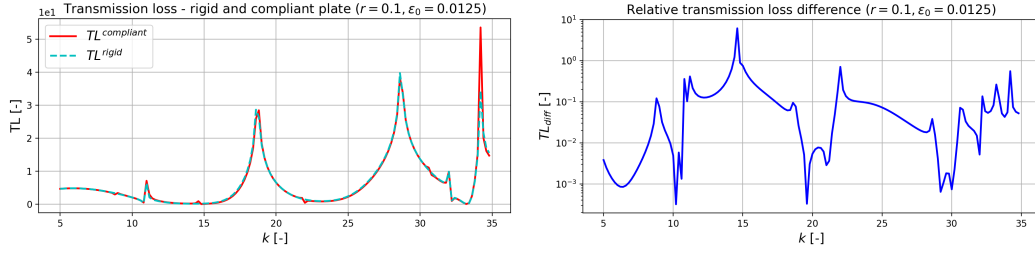


Figure 13: Relative difference of the transmission loss values for the rigid and compliant plate, $r = 0.1\varepsilon_0$ m, $N = 24$.

zero Neumann condition applies. The plate represented by interface Γ_0 is anchored in the waveguide walls, so that quantities $\mathbf{u} = 0$ and $\boldsymbol{\theta} = 0$ on $\partial\Gamma_0$. Also the same acoustic fluid and the same elastic solid are considered, as in the validation tests. The heterogeneous structure – the plate perforations – are specified by the circular holes with $r = 0.1\varepsilon_0$ m, whereby $\varepsilon_0 = 0.0025$, which corresponds to the number $N = 120$ of holes (counted along the longer side of the plate).

The computed macroscopic responses are shown in Fig. 14 which depicts the acoustic pressure field \hat{P} in $\hat{\Omega}^+ \cup \hat{\Omega}^-$ and the distributions of the following quantities defined in the interface Γ_0 : the “in-layer” pressure p^0 , the plate deflection u_3 and the plate rotations $\boldsymbol{\theta} = (\theta_1, \theta_2)$.

7. Conclusion

In this paper, we derive transmission conditions which serve for coupling acoustic fluid pressure fields on an interface which represents a compliant perforated elastic plate. For this, we consider a fictitious layer which embeds the elastic plate with periodic perforation, such that the perforation period is proportional to the layer and plate thicknesses. To derive the transmission conditions, the layer is decoupled from the “outer” acoustic field which is respected by introducing Neumann fluxes (the acoustic momentum). The layer is then treated by the asymptotic analysis based on the periodic unfolding homogenization method. As the result, the layer reduces to the 2D planar manifold Γ_0 where the homogenized model presents a coupled system of PDEs governing the “in-layer” variables: the mean pressure field and the plate deflection and rotations. Further averaging procedure based on a weighted integration in the transversal direction w.r.t. the layer mid-plane yields additional relationships which enable us to couple the “outer” acoustic field with the “in-layer” variables. In this way, the Dirichlet-to-Neumann operator is constructed which couples traces of the “outer” acoustic pressure

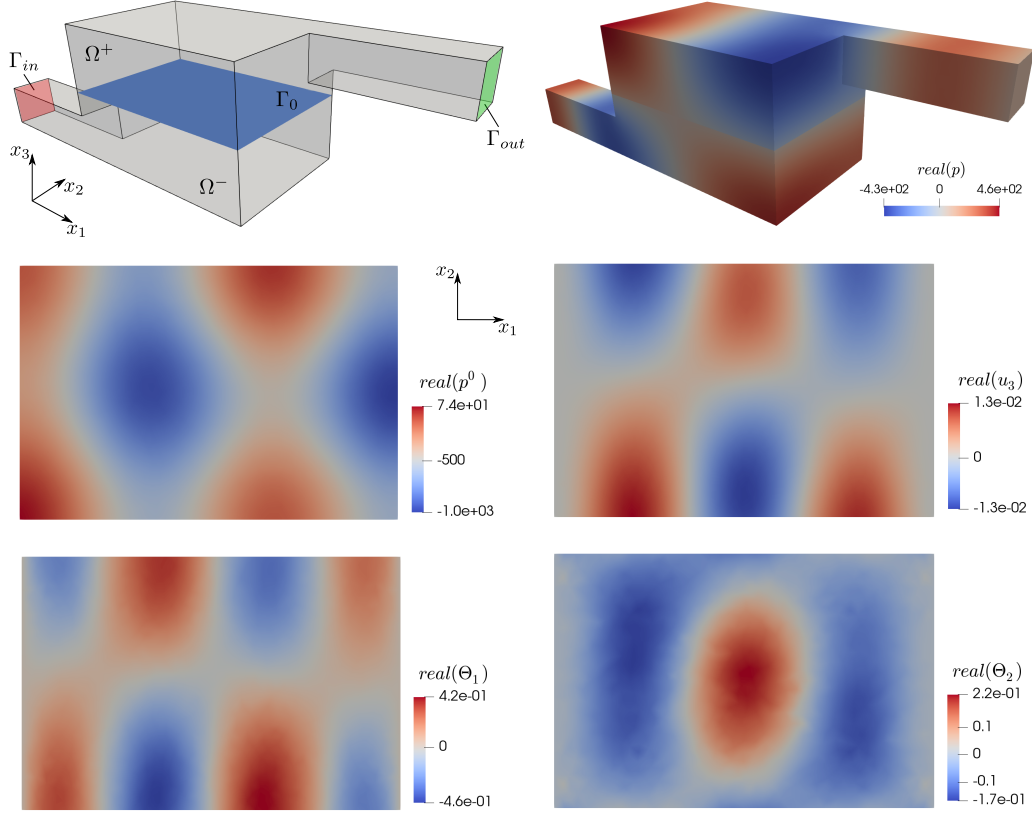


Figure 14: Acoustic pressure fields and plate deformations induced by the incident wave prescribed at the inlet of the waveguide. The plate periodic perforation is characterized by the hole radius, $r = 0.1\varepsilon_0$ m, where $\varepsilon_0 = 0.0025$.

with its normal-projected derivatives on both sides of the interface.

The numerical examples reported here illustrate the validation tests which have been performed to explore the modelling errors associated with the homogenization and the “3D-to-2D” dimension reduction of the layer which is replaced by the interface coupling conditions. We used the circular shape of holes, however, arbitrary shaped cylindrical holes can be considered. The validation tests were based on the comparison of responses computed using the homogenized models with the corresponding responses of reference model, here presented by direct numerical simulations (DNS) of the non-homogenized vibroacoustic problem. In these test, the convergence $\varepsilon \rightarrow 0$ was examined by increasing the number of the periods with proportionally smaller holes. It has been demonstrated that for a sufficiently small ε_0 , justifying the scale separation, numerical results obtained using the homogenized vibroacoustic model are quite close to the corresponding results of the DNS. This observation underlines the main advantage of the homogenized model:

it provides very good approximation of the reference solution, but at a considerably lower computational cost than the DNS solution. To illustrate the computational effort reduction, in the presented examples, the piecewise linear FE approximation of the homogenized problem has only about 2×10^4 degrees of freedom (DOFs) at the macroscopic level, whereas the microscopic subproblems are solved each with about 1.5×10^4 DOFs to get the homogenized coefficients. To compute relevant results even for much simpler geometry employed in the validation test, the DNS requires more than 2×10^5 DOFs for the approximation of the acoustic field in the layer and about the similar number of DOFs for the compliant elastic structure.

Among the topics of the future research, the homogenization-based modelling of the compliant plate with arbitrarily shaped periodic perforations presents one of the most interesting issues since such structures provide significantly bigger potential to modify the vibroacoustic transmission. First steps towards optimal design of perforated plates in the acoustic transmission problems were reported in [15, 16].

Acknowledgment. This research was supported by project GACR 17-01618S of the Scientific Foundation of the Czech Republic and due to the European Regional Development Fund-Project “Application of Modern Technologies in Medicine and Industry” (No. CZ.02.1.01/0.0/ 0.0/17 048/0007280), and in part by project LO 1506 of the Czech Ministry of Education, Youth and Sports.

A. Appendix

A.1. *A priori estimates*

To derive the *a priori* estimates on the solution of the problem (20)-(21), we substitute there $q^\varepsilon = p^\varepsilon$, $\mathbf{v}^\varepsilon = \mathbf{u}^\varepsilon$, $v_3 = u_3$ and $\boldsymbol{\theta}^\varepsilon = \boldsymbol{\vartheta}^\varepsilon$. Cosequently, upon obvious division of the two equations by \bar{h} and ρ_0 , respectively, and summation the resulting identities we get

$$\begin{aligned} & -\omega^2 \int_{\Gamma^\varepsilon} \frac{\rho_S}{\rho_0} \left[|\mathbf{u}^\varepsilon|^2 + \frac{h^2}{12} |\boldsymbol{\theta}^\varepsilon|^2 \right] - \frac{\omega^2}{c^2 \bar{h}} \int_{\hat{\Omega}^{*\varepsilon}} |p^\varepsilon|^2 \\ & + \frac{h^2}{12 \rho_0} \int_{\Gamma^\varepsilon} \mathbb{E}^\varepsilon \bar{\nabla}^S \boldsymbol{\theta}^\varepsilon : \bar{\nabla}^S \boldsymbol{\theta}^\varepsilon + \frac{1}{\rho_0} \int_{\Gamma^\varepsilon} \mathbb{E}^\varepsilon \bar{\nabla}^S \bar{\mathbf{u}}^\varepsilon : \bar{\nabla}^S \bar{\mathbf{u}}^\varepsilon \\ & + \frac{1}{\rho_0} \int_{\Gamma^\varepsilon} \varsigma^\varepsilon |\bar{\nabla} u_3^\varepsilon - \boldsymbol{\theta}^\varepsilon|^2 + \frac{1}{\bar{h}} \int_{\hat{\Omega}^{*\varepsilon}} |\hat{\nabla} p^\varepsilon|^2 = -\frac{i\omega}{\varepsilon \bar{h}} \int_{\Gamma_\delta^\pm} g^{\varepsilon \pm} p^\varepsilon. \end{aligned} \quad (83)$$

Note that, due to the above substitution of the test functions in (20)-(21), the r.h.s. interaction terms expressed in terms of the integrals on $\partial_\circ \Gamma^\varepsilon$ and Γ^ε

vanish upon the summation of the two equalities. Using the assumption on the elastic constants \mathbb{E}^ε , $\mathbf{S}^\varepsilon = \varsigma^\varepsilon \mathbf{I}$, there exist constants c_E and c_ς (independent of ε), such that we get

$$\begin{aligned} & \left[\frac{h^2}{12\rho_0} c_E \left\| \bar{\nabla}^S \boldsymbol{\theta}^\varepsilon \right\|_{L^2(\Gamma^\varepsilon)}^2 + \frac{1}{\rho_0} (c_E \left\| \bar{\nabla}^S \bar{\mathbf{u}}^\varepsilon \right\|_{[L^2(\Gamma^\varepsilon)]^2}^2 + c_\varsigma \left\| \bar{\nabla} u_3^\varepsilon - \boldsymbol{\theta}^\varepsilon \right\|_{[L^2(\Gamma^\varepsilon)]^2}^2) \right] \\ & + \frac{1}{h} \int_{\hat{\Omega}^{*\varepsilon}} |\hat{\nabla} p^\varepsilon|^2 \leq \omega^2 \frac{\bar{\rho}_S}{\rho_0} \left(\|u_3^\varepsilon\|_{L^2(\Gamma^\varepsilon)} + \|\bar{\mathbf{u}}^\varepsilon\|_{[L^2(\Gamma^\varepsilon)]^2} + \frac{h^2}{12} \|\boldsymbol{\theta}^\varepsilon\|_{[L^2(\Gamma^\varepsilon)]^2}^2 \right) \\ & + \frac{\omega^2}{c^2 \bar{h}} \|p^\varepsilon\|_{L^2(\hat{\Omega}^{*\varepsilon})}^2 + \frac{\omega}{\varepsilon \bar{h}} \left| \int_{\Gamma^\pm} \hat{g}^{\varepsilon\pm} p^\varepsilon \right|. \end{aligned} \quad (84)$$

To estimate the last r.h.s. integral, we use the unfolding operation, see *e.g.* [4], and a smooth extension \tilde{p} from $\hat{\Omega}^{*\varepsilon}$ to whole $\hat{\Omega}$, *i.e.*, for unfolded functions, there is an extension from Y^* to whole Y . For any $p \in H^1(\Omega^\varepsilon)$ there exists $\tilde{p} \in H^1(\Omega)$ such that $\tilde{p} - p = 0$ in Ω^ε and the following estimates hold:

$$\begin{aligned} \left\| \tilde{p} - \int_{\Omega} \tilde{p} \right\|_{L^2(\hat{\Omega})} & \leq C \|\nabla \tilde{p}\|_{[L^2(\hat{\Omega})]^3} , \\ \|\nabla \tilde{p}\|_{[L^2(\hat{\Omega})]^3} & \leq C \|\nabla p\|_{[L^2(\hat{\Omega}^{*\varepsilon})]^3} . \end{aligned} \quad (85)$$

The trace theorem yields the following modification of the Poincaré–Wirtinger inequality: for any $f \in H^1(Y)$

$$\|f - \mathcal{M}_Y(f)\|_{L^2(\partial Y)} \leq C \|\nabla_y f\|_{L^2(Y)} . \quad (86)$$

Let us define

$$G^\varepsilon(x') = \oint_{I_y^\pm} \mathcal{T}_\varepsilon(g^{\varepsilon\pm})(x', y') \, dy' , \quad x' \in \Gamma_0 . \quad (87)$$

Now, we can now estimate the last r.h.s. integral in (84),

$$\begin{aligned}
& \frac{1}{\varepsilon} \left| \int_{\Gamma^\pm} \hat{g}^{\varepsilon\pm} p^\varepsilon \right| = \frac{1}{\varepsilon} \int_{\Gamma_0} \oint_{I_y^\pm} |\mathcal{T}_\varepsilon(\hat{g}^{\varepsilon\pm} p^\varepsilon)| \\
& \leq \frac{1}{\varepsilon} \int_{\Gamma_0} |\mathcal{M}_Y^\varepsilon(\mathcal{T}_\varepsilon(p^\varepsilon))| \oint_{I_y^\pm} |\mathcal{T}_\varepsilon(\hat{g}^{\varepsilon\pm})| \\
& \quad + \frac{1}{\varepsilon} \left(\int_{\Gamma_0} \oint_{I_y^\pm} |\mathcal{T}_\varepsilon(p^\varepsilon) - \mathcal{M}_Y^\varepsilon(\mathcal{T}_\varepsilon(p^\varepsilon))|^2 \right)^{1/2} \left(\int_{\Gamma_0} \oint_{I_y^\pm} |\mathcal{T}_\varepsilon(\hat{g}^{\varepsilon\pm})|^2 \right)^{1/2} \\
& \leq C' \|p^\varepsilon\|_{L^2(\hat{\Omega}^{\varepsilon\pm})} \left\| \frac{1}{\varepsilon} G^\varepsilon \right\|_{L^2(\Gamma)} + \frac{C_Y}{\varepsilon} \left(\int_{\Gamma_0} \oint_Y |\nabla_y \mathcal{T}_\varepsilon(\tilde{p}^\varepsilon)|^2 \right)^{1/2} \|g^{\varepsilon\pm}\|_{L^2(\Gamma_\delta^\pm)} \\
& \leq C' \|p^\varepsilon\|_{L^2(\hat{\Omega}^{\varepsilon\pm})} \left\| \frac{1}{\varepsilon} G^\varepsilon \right\|_{L^2(\Gamma)} + C \left(\int_{\Omega} |\hat{\nabla}_x \tilde{p}^\varepsilon|^2 \right)^{1/2} \|\hat{g}^{\varepsilon\pm}\|_{L^2(\Gamma_\delta^\pm)} \\
& \leq C' \|p^\varepsilon\|_{L^2(\hat{\Omega}^{\varepsilon\pm})} \left\| \frac{1}{\varepsilon} G^\varepsilon \right\|_{L^2(\Gamma)} + C \left\| \hat{\nabla}_x p^\varepsilon \right\|_{[L^2(\hat{\Omega})]^3} \|\hat{g}^{\varepsilon\pm}\|_{L^2(\Gamma_\delta^\pm)} ,
\end{aligned} \tag{88}$$

where all the positive constants C, C', C_Y are independent of ε . Due to the assumed form of the fluxes $\hat{g}^{\varepsilon\pm}$ given by (22) and assuming the bounded solution $(p^\varepsilon, \mathbf{u}^\varepsilon, \boldsymbol{\theta}^\varepsilon)$ in the L^2 norms, (84) with (88) yields the desired estimates on the gradients of the solution, see the Theorem 1.

A.2. Reconstruction of responses at microlevel

The two-scale field reconstruction of the homogenized model response is based on the coordinate split related to the periodic lattice. For $\varepsilon_0 > 0$, using the rescaled cell Z^{ε_0} we introduce its local copies Z^{K, ε_0} labeled by index K whereby $\{\bar{x}^K\}_K$ is the set of centers $\bar{x}^K \in \Gamma_0$ of each Z^{K, ε_0} . For the sake of simplicity, we consider only such domains Γ_0 for which the transmission layers Ω^{δ_0} are generated as a union of non overlapping Z^{K, ε_0} , thus (recall that \bar{Z} is the closure of Z)

$$\overline{\Omega^{\delta_0}} = \bigcup_{K \in \mathcal{J}_\Omega^{\delta_0}} \overline{Z^{K, \varepsilon_0}} , \quad Z^{K, \varepsilon_0} = Z^{\varepsilon_0} + \boldsymbol{\xi}^K , \tag{89}$$

where $\mathcal{J}_\Omega^{\delta_0}$ is the set of indices K associated to the lattice vector $\mathbf{k} = (k_i) \in \mathbb{Z}^2$ such that $\boldsymbol{\xi}^K = \varepsilon_0 k_i a_i$, recalling the definition $Y = \prod_i] -a_i/2, a_i/2[$ and $|Y| = 1$.

For any global position $x \in Z^{K, \varepsilon_0}$, the local “mesoscopic” coordinate

$$y = (x - \bar{x}^K)/\varepsilon_0 , \tag{90}$$

can be introduced, such that $y \in Y$. The folding procedure can be summarized, as follows: for each “real sized” cell Z^{K,ε_0} with its center $\bar{x}^K \in \Gamma_0$ evaluate the local responses given below as two-scale functions $f(x', y)$, where $(x', y/\varepsilon_0) \in Z^{K,\varepsilon_0}$, thus, $y \in Y$ is given, as described above. In what follows, we drop the index K labelling the copy of the local cell.

Due to the homogenization result, by virtue of the characteristic responses, it is possible to reconstruct the acoustic pressure in the fictitious transmission layer. For this we use the truncated expansion (31), where $p^1(x', y)$ depends on $\bar{\nabla}_x p^0$, g^0 , and \mathbf{u}^0 through (43). Thus, for a given plate thickness $h = \varepsilon_0 \bar{h}$ yielding ε_0 , the acoustic pressure field in $Z^{*,\varepsilon_0}(\varepsilon_0[x'/\varepsilon_0]_\Xi) = \varepsilon_0 Y^* + \mathbf{k}\varepsilon_0$, $\mathbf{k} = (k_1, k_2) \in \mathbb{Z}^2$ which is the local copy of $\varepsilon_0 Y^*$ placed at $x' \in \Gamma_0$, is given as follows,

$$\begin{aligned} p^{\varepsilon_0} &\approx p^0(x') + \varepsilon_0 p^1(x', y), \quad \text{where} \\ p^1(x', y) &= \pi^\beta(y) \partial_\beta^x p^0(x') + i\omega \xi(y) g^0(x') + i\omega \eta^k(y) u_k^0(x') \\ &= \pi^\beta(y) \frac{1}{2} \partial_\beta^x (\hat{P}^+(x') + \hat{P}^-(x')) + i\omega \xi(y) \frac{1}{2} (\hat{G}_0^+(x') + \hat{G}_0^-(x')) + i\omega \eta^k(y) u_k^0(x'), \end{aligned} \tag{91}$$

where $y = (y', z) \in Y^*$. We recall that p^0 and g^0 are expressed in terms of the global fields \hat{P}^\pm and \hat{G}_0^\pm according to (67)₂ and (75)₁. It is worth noting, that the position $x' \in \Gamma_0 \cap Z^{*,\varepsilon_0}(\varepsilon_0[x'/\varepsilon_0]_\Xi)$ varies and y is determined by (90).

References

- [1] A.S. Bonnet-Bendhia, D. Drissi, and N. Gmati. Mathematical analysis of the acoustic diffraction by a muffler containing perforated ducts. *Math. Models and Methods in Appl. Sci.*, 15(7):1059–1090, 2005.
- [2] R. Cimrman, V. Lukeš, and E. Rohan. Multiscale finite element calculations in python using sfepy. *Advances in Computational Mathematics*, 2019. Accepted for publication.
- [3] A. Cioranescu, D. Damlamian, G. Griso, and D. Onofrei. The periodic unfolding method for perforated domains and neumann sieve models. *Journal de Mathématiques Pures et Appliquées*, 89(3):248–277, 2008.
- [4] D. Cioranescu, A. Damlamian, and G. Griso. The periodic unfolding method in homogenization. *SIAM Journal on Mathematical Analysis*, 40(4):1585–1620, 2008.

- [5] Xavier Claeys and Bérangère Delourme. High order asymptotics for wave propagation across thin periodic interfaces. *Asymptotic Analysis*, pages 35–82, 2013.
- [6] Bérangère Delourme, Housseem Haddar, and Patrick Joly. Approximate models for wave propagation across thin periodic interfaces. *Journal de Mathématiques Pures et Appliquées*, 98(1):28 – 71, 2012.
- [7] Christina Dörlemann, Martin Heida, and Ben Schweizer. Transmission conditions for the helmholtz-equation in perforated domains. *Vietnam Journal of Mathematics*, 45(1):241–253, 2017.
- [8] S. S. Jung and et.al. Sound absorption of micro-perforated panel. *Journal of the Korean Physical Society*, 50:1044–1051, 2007.
- [9] Yu Liu and Chuanbo He. Analytical modelling of acoustic transmission across double-wall sandwich shells: Effect of an air gap flow. *Composite Structures*, 136:149 – 161, 2016.
- [10] Jean-Jacques Marigo and Agnès Maurel. Homogenization models for thin rigid structured surfaces and films. *J. Acoust. Soc. Am.*, 140(1):260–273, 2016.
- [11] Jean-Jacques Marigo and Agnès Maurel. Two-scale homogenization to determine effective parameters of thin metallic-structured films. *Proceedings of the Royal Society of London A: Mathematical, Physical and Engineering Sciences*, 472(2192), 2016.
- [12] L. Maxit, C. Yang, L. Cheng, and J.-L. Guyader. Modeling of micro-perforated panels in a complex vibro-acoustic environment using patch transfer function approach. *Acoustical Society of America Journal*, 131:2118, 2012.
- [13] E. Rohan, R. Cimrman, and B. Miara. Modelling response of phononic Reissner-Mindlin plates using a spectral decomposition. *Appl. Math. Comput.*, 258:617–630, may 2015.
- [14] E. Rohan and V. Lukeš. Homogenization of the acoustic transmission through perforated layer. *J. of Comput. and Appl. Math.*, 234:1876–1885, 2010.
- [15] E. Rohan and V. Lukeš. Sensitivity analysis for optimal design of perforated plates in vibro-acoustics: homogenization approach. In *Proceedings of ISMA 2012 – USD 2012*, pages 4201–4214. KU Leuven, 2012.

- [16] E. Rohan and V. Lukeš. Homogenized perforated interface in acoustic wave propagation – modeling and optimization. In Z. Dimitrovová et.al., editor, *Proc. of the 11th International Conference on Vibration Problems, ICOVP 2013*, pages 1–10, Lisbon, Portugal, 2013.
- [17] E. Rohan and B. Miara. Band gaps and vibration of strongly heterogeneous Reissner-Mindlin elastic plates. *Comptes Rendus Mathématique*, 349:777–781, 2011.
- [18] Eduard Rohan and Bernadette Miara. Elastodynamics of strongly heterogeneous periodic plates using Reissner-Mindlin and Kirchhoff-Love models. *ZAMM - J. Appl. Math. Mech. / Zeitschrift für Angew. Math. und Mech.*, 96(3):304–326, mar 2016.
- [19] K. Sakagami, K. Matsutani, and M. Morimoto. Sound absorption of a double-leaf micro-perforated panel with an air-back cavity and a rigid-back wall: Detailed analysis with a helmholtz-kirchhoff integral formulation. *Applied Acoustics*, 71:411–417, 2010.
- [20] F.-A. Stremtan and I. Lupea. Assessing the sound absorption of micro-perforated panels by using the transfer function and the impedance tube. *RJAV*, IX(2):94–99, 2012. ISSN 1584-7284.
- [21] D. Takahashi and M. Tanaka. Flexural vibration of perforated plates and porous elastic materials under acoustic loading. *The Journal of the Acoustical Society of America*, 112(4):1456–1464, 2002.
- [22] M. Toyoda and D Takahashi. Reduction of acoustic radiation by impedance control with a perforated absorber system. *Journal of Sound and Vibration*, 286:601–614, 2005.
- [23] J. Zhou, A. Bhaskar, and X. Zhang. Sound transmission through a double-panel construction lined with poroelastic material in the presence of mean flow. *Journal of Sound and Vibration*, 332:3724–3734, 2013.